Cooperative visibility maintenance for leader-follower formations in obstacle environments

Dimitra Panagou, *Member, IEEE,* and Vijay Kumar, *Fellow, IEEE*

***Abstract*—Vision-based formation control of multiple agents, such as mobile robots or fully-autonomous cars, has recently received great interest due to its application in robotic networks and automated highways. This paper addresses the cooperative motion coordination of leader-follower formations of nonholonomic mobile robots, under visibility and communication constraints in known polygonal obstacle environments. We initially consider the case of $\mathbf{N} = 2$ agents moving in $\mathrm{L}-\mathrm{F}$ fashion and propose a feedback control strategy under which L ensures obstacle avoidance for both robots, while F ensures visibility maintenance with L and inter-vehicle collision avoidance. The derived algorithms are based on: set-theoretic methods to guarantee visibility maintenance, dipolar vector fields to maintain the formation shape, and the consideration of the formation as a tractor-trailer system to ensure obstacle avoidance. We furthermore show how the coordination and control design extends to the case of $\mathbf{N} > 2$ agents, and provide simulation results which demonstrate the efficacy of the control solutions. The proposed algorithms do not require information exchange among robots, but are instead based on information locally available to each agent. In this way, the desired tasks are executed and achieved in a decentralized manner, with each robot taking care of converging to a desired configuration, while maintaining visibility with its target.**

***Index Terms*—Path Planning for Multiple Mobile Robot Systems, Nonholonomic Motion Planning, Leader-Follower Formations, Visibility Maintenance**

I. Introduction

Control of Leader $-$ Follower $(\mathrm{L}-\mathrm{F})$ formations of autonomous vehicles and robots has seen an increasing interest during the past few years. Research in this area has in part been stimulated by the recent technological advances in communication and computation, which have allowed for the development of multi-agent systems that accomplish collaborative tasks in an effective, robust and reliable fashion. Within the field of mobile robotics, $\mathrm{L}-\mathrm{F}$ formations arise in various applications, from surveillance and monitoring to exploration and coverage. From a practical point-of-view, the case when robots are subject to limited sensing and communication is of particular interest. For instance, mobile robots operating indoors typically lack access to global positioning measurements, while information exchange is either restricted or obstructed by physical obstacles. Such limitations impose various types of constraints to each robot, which naturally extend to the whole multi-robot system. For the desired tasks to be fulfilled, these constraints should be taken into account during the motion planning, coordination and control design.

Vision-based sensing and localization has recently become a popular and versatile means of controlling robot formations. The authors in [1], [2] consider the cooperative formation control of mobile robots and propose switching solutions which change the formation shape, so that obstacle avoidance is achieved. In [3] the authors approach the formation maintenance for nonholonomic mobile robots as a visual servoing task for each one of the followers; the proposed solutions, based on either the concept of Navigation Functions, or on the locally linearized system dynamics, yield Leader-to-Formation stability [4]. Vision-based localization, along with controllers based on input-output linearization, for a formation of mobile robots is addressed in [5], [6]. Vision-based controls for similar formation tasks are also proposed in [7]–[9].

The common underlying assumption in the aforementioned contributions is that the robots have omnidirectional (or pan-controlled) cameras, and that the linear and angular velocities of L are either communicated to, or estimated by F. However, when communication between robots is absent and/or their on-board sensors have limited capabilities (e.g. limited range and angle-of-view), then the robots can typically stay connected if and only if L is always visible to F. The latter specification imposes a set of *visibility constraints* which should never be violated, so that F always maintains visibility with L.

Formation control under visibility constraints exhibits similarities in terms of problem formulation to the control design for a nonholonomic robot with field-of-view constraints which needs to maintain visibility with a target, e.g. a fixed landmark or an evader. For the fixed target case, hybrid control strategies are presented in [10], [11], whereas optimal paths which respect the field-of-view constraints are computed in [12], [13]. In [14] visibility maintenance for a chain of Dubins-like vehicles is addressed based on the notion of controlled invariance. In [15], [16] the authors use a game-theoretic formulation for the problem of tracking an omnidirectional evader with a nonholonomic mobile pursuer of bounded speed. These contributions, albeit significant and elegant, do not consider the presence of physical obstacles.

Maintaining visibility in polygonal obstacle environments has been mostly addressed with game-theoretic strategies for one pursuer (observer) tracking one evader (target) in an antagonistic fashion, see [17]–[20] and the references therein.

The authors gratefully acknowledge the support from ONR Grant N00014-07-1-0829, ONR MURI Grant N00014-08-1-0696, NSF 1138847, ARL Grant W911NF-08-2-0004, ONR Grant N00014-09-1-1031, ONR Grant N00014-09-1-1051, NSF IIS-1328805. This work was supported in part by TerraSwarm, one of six centers of STARnet, a Semiconductor Research Corporation program sponsored by MARCO and DARPA.

Dimitra Panagou is with the Coordinated Science Laboratory, College of Engineering, University of Illinois at Urbana-Champaign, Urbana, IL, USA dpanagou@illinois.edu.

Vijay Kumar is with the GRASP Lab, School of Engineering and Applied Sciences, University of Pennsylvania, Philadelphia, PA, USA, kumar@seas.upenn.edu

The corresponding optimal control problems are defined in terms of either the shortest path, or the minimum time, for the evader to escape the visibility region of the observer. In [18], [20] the authors further discuss the applicability of the derived motion strategies in cooperative leader-following scenarios for mobile robots; in these cases, the follower is assumed to have full access on the leader's configuration and velocities.

A. Problem Overview and Organization

This paper considers the cooperative motion coordination of $\mathrm{N} \geq 2$ mobile robots with unicycle kinematics in known obstacle environments, using vision-based formation control. This problem is relevant to various multi-agent applications, including the exploration and surveillance of cluttered environments with multiple robots of minimal sensing and communication capabilities, as well as the navigation of autonomous vehicle platoons towards fully automated highways.

The robots are assumed to move in $\mathrm{L}-\mathrm{F}$ *formation* under visibility and communication constraints in the following sense: Every robot i (except the leader of the formation) can see at least one other robot j; we refer to a robot j being visible from another robot i as a $\mathrm{L}-\mathrm{F}$ *pair*. The onboard sensor systems are of limited range and limited angle-of-view, defining thus a cone-of-view for each robot. We assume that robot i is localized with respect to (w.r.t.) robot j if and only if j belongs into the cone-of-view of i. We also assume that communication among robots for exchanging information is not available. Thus, robots j and i can move as a $\mathrm{L}-\mathrm{F}$ pair if and only if j is always visible from i, or in other words, if and only if i always maintains visibility with j. The safe and reliable navigation of the robots furthermore dictates that inter-vehicle collisions and physical obstacles should always be avoided. Consequently, *the motion coordination and control problem for the multi-robot system reduces into guaranteeing that the objectives of visibility maintenance, collision/obstacle avoidance and convergence to desired goals are always accomplished*.

To this end, we initially consider $\mathrm{N} = 2$ agents moving as a $\mathrm{L}-\mathrm{F}$ pair and propose a motion coordination and control strategy, in which L is responsible for ensuring obstacle avoidance for both robots while navigating towards a goal configuration, and F is responsible for ensuring visibility maintenance with L and inter-vehicle collision avoidance. This strategy can be described as follows:

1) The first level involves the motion planning and control design for F (Section III). Inspired by set-theoretic control methods and notions from viability theory [21], we provide the necessary and sufficient conditions for visibility maintenance in obstacle-free environments. We also propose a state feedback control scheme for F which guarantees visibility maintenance and collision avoidance w.r.t. L, based on dipolar vector fields [22].
2) The second level involves the motion planning and control design for the L-F formation in a known obstacle environment, given a cell decomposition of the free space and a high-level discrete motion plan for L (Section IV). Inspired by the tractor-pulling-trailer paradigm [23] we propose a hybrid feedback motion plan for L, which guarantees obstacle avoidance for both robots. We furthermore extend this idea and control design to the case of chain formations with $\mathrm{N} > 2$ robots.

Our motion coordination and control design is characterized as cooperative, in the sense that the robots are not thought of as antagonistic pairs of one pursuer, one evader, with the latter trying to escape the sensing area of the former, but on the contrary are controlled so that each one always keeps its target visible in its sensing area. The proposed algorithms do not require communication between the robots regarding on their states, but are instead based on information locally available to each agent; only the upper bounds of the velocities of L are assumed to be a priori known to F. In this way, the tasks are executed in a decentralized manner, with each robot taking care of converging to a desired configuration, while maintaining visibility with its target. More specifically: on one hand, F is localized w.r.t. L yet is aware neither of its navigation plan, nor of its velocities at each time instant. On the other hand, L is not aware of the state of F, yet its motion ensures that both robots avoid physical obstacles. The same logic applies also in chain formations of $\mathrm{N} > 2$ agents. The efficacy of our algorithms is demonstrated and evaluated through simulation results in Section V, while Section VI concludes the paper and presents our ideas on future extensions of this work.

B. Contributions

To the best of our knowledge, this paper is the first contribution addressing the cooperative formation control of *multiple robots in obstacle environments under sensing (visibility) and communication constraints, with guaranteed visibility and safety maintenance*. The proposed state feedback control strategy ensures the safe navigation of the multi-robot formation in known cluttered environments, using minimal vision-based information only and without the need for exchanging or estimating velocities online. More specifically:

Compared to earlier work on vision-based formation control in obstacle environments [1], [2], our method does not require communication between robots, or state estimation algorithms. Moreover, the onboard cameras are not assumed to be omnidirectional or pan-controlled, but rather fixed and of limited range and field-of-view. Finally, the consideration of the tractor-trailer paradigm guarantees obstacle avoidance for the formation via a hybrid control strategy for L only, whereas in [1], [2] the formation switching is based on a coordination protocol involving information on the states of all robots.

The differences of our approach compared to other vision-based formation control strategies [5]–[9] rely on the absence of communication, the consideration of limited field-of-view and range constraints, as well as the consideration of physical obstacles. The latter specification is the main difference of the current paper compared to other papers on maintaining visibility problems involving robots with field-of-view constraints [10]–[16]. Finally, compared to [18], [20], here F is not required to have full access on the state vector of L.

Part of this work has appeared in [24]. The current paper additionally includes: (i) the proofs verifying the correctness

of our control strategy, which were omitted in the conference paper in the interest of space, and (ii) its extension for $\mathrm{N} > 2$ robots, along with illustrative simulation results. Finally, compared to our recent work in [25], this paper is different in the following aspects: Here, we consider a multi-agent scenario in the presence of physical obstacles, while the problem addressed in [25] considers neither multiple robots, nor physical obstacles. Consequently, the current paper differs in the adopted system modeling, considered constraints and the derived control strategy.

II. Mathematical Modeling

A. Leader-Follower Kinematics

We first consider the case of $\mathrm{N} = 2$ unicycle mobile robots moving in $\mathrm{L}-\mathrm{F}$ formation. The motion of each one of the robots L, F w.r.t. a global frame $\mathcal{G}$ is described by:

$$\dot{\boldsymbol{q}}_{\boldsymbol{i}} = \boldsymbol{G}(\boldsymbol{q}_{\boldsymbol{i}})\boldsymbol{v}_{\boldsymbol{i}} \Rightarrow \begin{bmatrix} \dot{x}_i \\ \dot{y}_i \\ \dot{\theta}_i \end{bmatrix} = \begin{bmatrix} \cos\theta_i & 0 \\ \sin\theta_i & 0 \\ 0 & 1 \end{bmatrix} \begin{bmatrix} u_i \\ w_i \end{bmatrix}, \tag{1}$$

where $i \in \{\mathrm{L}, \mathrm{F}\}$, $\boldsymbol{q}_{\boldsymbol{i}} = \begin{bmatrix} x_i & y_i & \theta_i \end{bmatrix}^\top$ is the configuration vector of robot i, $\boldsymbol{r}_{\boldsymbol{i}} = \begin{bmatrix} x_i & y_i \end{bmatrix}^\top$ is the position vector and θ_i is the orientation of i w.r.t. frame $\mathcal{G}$, u_i, w_i are the linear and angular velocity of i in the body-fixed frame $\mathcal{I} \in \{\mathcal{L}, \mathcal{F}\}$, with $\mathcal{L}$ being the leader frame and $\mathcal{F}$ being the follower frame.

To describe the motion of F w.r.t. the leader frame $\mathcal{L}$, consider the position vector $\boldsymbol{r} = \begin{bmatrix} x & y \end{bmatrix}^\top$ of F w.r.t. $\mathcal{L}$, given as $\boldsymbol{r} = \mathbf{R}(-\theta_\mathrm{L})\,(\boldsymbol{r}_\mathbf{F} - \boldsymbol{r}_\mathbf{L})$, and take the time derivative as:

$$\dot{\boldsymbol{r}} = \dot{\mathbf{R}}(-\theta_\mathrm{L})\,(\boldsymbol{r}_\mathbf{F} - \boldsymbol{r}_\mathbf{L}) + \mathbf{R}(-\theta_\mathrm{L})\,(\dot{\boldsymbol{r}}_\mathbf{F} - \dot{\boldsymbol{r}}_\mathbf{L}), \tag{2}$$

where

$$\mathbf{R}(-\theta_\mathrm{L}) = \begin{bmatrix} \cos(-\theta_\mathrm{L}) & -\sin(-\theta_\mathrm{L}) \\ \sin(-\theta_\mathrm{L}) & \cos(-\theta_\mathrm{L}) \end{bmatrix} = \begin{bmatrix} \cos\theta_\mathrm{L} & \sin\theta_\mathrm{L} \\ -\sin\theta_\mathrm{L} & \cos\theta_\mathrm{L} \end{bmatrix} \tag{3}$$

is the rotation matrix of the frame $\mathcal{L}$ w.r.t. frame $\mathcal{G}$, and

$$\dot{\mathbf{R}}(-\theta_\mathrm{L}) = \begin{bmatrix} 0 & w_\mathrm{L} \\ -w_\mathrm{L} & 0 \end{bmatrix} \mathbf{R}(-\theta_\mathrm{L}). \tag{4}$$

Substituting (3), (4), (1) into (2) and after some algebra one eventually gets:

$$\begin{bmatrix} \dot{x} \\ \dot{y} \end{bmatrix} = \begin{bmatrix} -1 & y \\ 0 & -x \end{bmatrix} \begin{bmatrix} u_\mathrm{L} \\ w_\mathrm{L} \end{bmatrix} + \begin{bmatrix} \cos(\theta_\mathrm{F} - \theta_\mathrm{L}) \\ \sin(\theta_\mathrm{F} - \theta_\mathrm{L}) \end{bmatrix} u_\mathrm{F}. \tag{5}$$

Define $\beta = \theta_\mathrm{F} - \theta_\mathrm{L}$; then differentiating w.r.t. time yields:

$$\dot{\beta} = \dot{\theta}_\mathrm{F} - \dot{\theta}_\mathrm{L} = w_\mathrm{F} - w_\mathrm{L}. \tag{6}$$

Combining equations (5) and (6) yields the system equations:

$$\begin{bmatrix} \dot{x} \\ \dot{y} \\ \dot{\beta} \end{bmatrix} = \underbrace{\begin{bmatrix} \cos\beta & 0 \\ \sin\beta & 0 \\ 0 & 1 \end{bmatrix} \begin{bmatrix} u_\mathrm{F} \\ w_\mathrm{F} \end{bmatrix}}_{\boldsymbol{f}(\boldsymbol{q},\boldsymbol{v}_\mathbf{F})} + \underbrace{\begin{bmatrix} -1 & y \\ 0 & -x \\ 0 & -1 \end{bmatrix} \begin{bmatrix} u_\mathrm{L} \\ w_\mathrm{L} \end{bmatrix}}_{\boldsymbol{g}(\boldsymbol{q},\boldsymbol{v}_\mathbf{L})}, \tag{7}$$

where $\boldsymbol{q} = \begin{bmatrix} x & y & \beta \end{bmatrix}^\top \in \mathcal{C} \subset \mathbb{R}^3$ is the state vector comprising the position $\boldsymbol{r} = \begin{bmatrix} x & y \end{bmatrix}^\top$ and the orientation β of the follower F w.r.t. the leader frame $\mathcal{L}$, $\mathcal{C}$ is the state space, $\boldsymbol{v}_\mathbf{F} = \begin{bmatrix} u_\mathrm{F} & w_\mathrm{F} \end{bmatrix}^\top \in \mathcal{U}_\mathrm{F}$ is the vector of control inputs, $\mathcal{U}_\mathrm{F} \subset \mathbb{R}^2$ is a compact set denoting the control space, and $\boldsymbol{g}(\boldsymbol{q}, \boldsymbol{v}_\mathbf{L})$ can be seen as a perturbation vector field, where $\boldsymbol{v}_\mathbf{L} = \begin{bmatrix} u_\mathrm{L} & w_\mathrm{L} \end{bmatrix}^\top \in \mathcal{U}_\mathrm{L} \subset \mathbb{R}^2$ is the vector of control inputs of L. The perturbation is vanishing if and only if $\boldsymbol{g}(\boldsymbol{q}, \boldsymbol{v}_\mathbf{L}) = \mathbf{0}$, which occurs if and only if $\boldsymbol{v}_\mathbf{L} = \mathbf{0}$. Consequently, the motion of L can be thought as a non-vanishing perturbation to the motion of F.

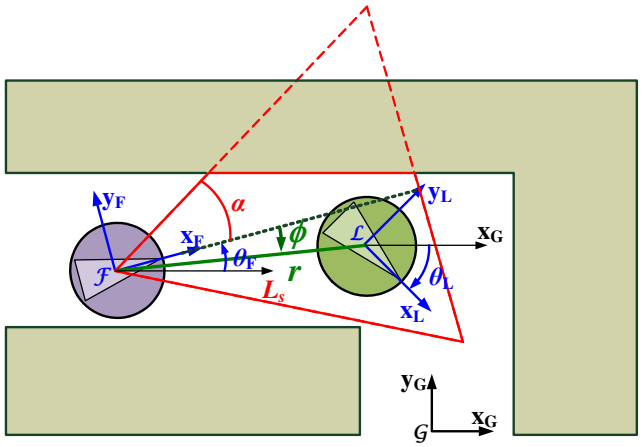

Fig. 1. The L-F setup in an environment with obstacles.

B. Modeling of the visibility constraints

We assume that F is equipped with a *fixed* onboard camera of limited angle-of-view $2\alpha < \pi$. Furthermore, we assume that F can reliably detect objects which lie within a limited region w.r.t. the forward-looking direction, as shown in Fig. 1. The limited sensing region is modeled as a cone-of-view for F, which essentially is an isosceles triangle in obstacle-free environments. Finally, we assume that F is localized w.r.t. L, i.e. that the distance $r = \sqrt{x^2 + y^2}$ and the bearing angle $\phi \in [-\alpha, \alpha]$ are measured.[1] Consequently, F can detect L if and only if L is in the cone-of-view, i.e. iff:

$$|\phi| \leq \alpha \;\text{ and }\; r \leq \frac{L_s \cos\alpha}{\cos\phi}, \tag{8}$$

where L_s is the length of the equal sides of the cone-of-view. These constraints define a closed subset K of $\mathcal{C}$, given as:

$$K = \{\boldsymbol{q} \in \mathcal{C} \mid h_k(\boldsymbol{q}) \leq 0,\; k = 1, 2\}, \tag{9}$$

where $h_1 = |\phi| - \alpha$ and $h_2 = r - \frac{L_s \cos\alpha}{\cos\phi}$, which we call the *visibility set* K. The set K includes every configuration $\boldsymbol{q} \in \mathcal{C}$ for which visibility is maintained. Controlling F, L so that the resulting trajectories $\boldsymbol{q}(t)$ never escape K, implies that visibility is always maintained.

Remark 1: Maintaining visibility for the $\mathrm{L}-\mathrm{F}$ formation described by (7) reduces thus into picking control inputs $\boldsymbol{v}_\mathbf{F} = \boldsymbol{\gamma}_\mathrm{F}(\cdot)$ for F, such that the visibility constraints (8) are met $\forall t \geq 0$, despite the non-vanishing perturbation $\boldsymbol{g}(\boldsymbol{q}, \boldsymbol{v}_\mathbf{L})$ induced by the control inputs $\boldsymbol{v}_\mathbf{L} = \boldsymbol{\gamma}_\mathrm{L}(\cdot)$ of L.

[1] This essentially implies that F measures its pose vector (position and orientation) w.r.t. frame $\mathcal{L}$, which can be done with techniques as in [7].

III. Visibility Maintaining Formation Control

Let us first consider the system (7) for L moving with some $u_{\mathrm{L}} \neq 0$, $w_{\mathrm{L}} \neq 0$, in an obstacle-free environment. As mentioned earlier, we assume that F is localized w.r.t. L, i.e. that F measures its position (x, y) and orientation β w.r.t. the leader frame $\mathcal{L}$. Yet, F does not have access to the navigation plan or the velocities $u_{\mathrm{L}}(t)$, $w_{\mathrm{L}}(t)$ of L at each time instant t. Thus, it is reasonable to assume that F has some a priori knowledge on the velocity bounds $u_{\mathrm{L}}^{\star}$, $w_{\mathrm{L}}^{\star}$ of L, in the sense that L is restricted to move with bounded velocities

$$0 \leq u_{\mathrm{L}} \leq u_{\mathrm{L}}^{\star}, \quad |w_{\mathrm{L}}| \leq w_{\mathrm{L}}^{\star}.$$

The task for F is to (ideally) keep a fixed distance r_d w.r.t. L with angle $\phi = 0$, where $2r_0 \leq r_d \leq L_s \cos\alpha$ and r_0 the radius of the robots; in that way, L gets centered in the field-of-view of F. This requirement specifies a manifold $\mathcal{M}$ of desired configurations $\boldsymbol{q_d} = \begin{bmatrix} x_d & y_d & \theta_d \end{bmatrix}^{\top}$ for F:

$$\mathcal{M} = \left\{ \boldsymbol{q_d} \in \mathcal{C} \;\middle|\; \begin{array}{c} {x_d}^2 + {y_d}^2 = {r_d}^2, \\ \theta_d = \mathrm{atan2}(y_d, x_d) + \mathrm{sign}(y_d)\pi \end{array} \right\}.$$

Thus, the control design for F reduces into finding a feedback control law $\boldsymbol{\gamma}_{\mathrm{F}}(\cdot)$ so that F converges to a configuration $\boldsymbol{q_d} \in \mathcal{M}$, with the trajectories $\boldsymbol{q}(t)$ always satisfying the visibility constraints (8).

However, since the perturbation $\boldsymbol{g}(\boldsymbol{q}, \boldsymbol{v_L})$ is non-vanishing $\forall \boldsymbol{q} \in \mathcal{C}$, none $\boldsymbol{q_d} \in \mathcal{M}$ is an equilibrium point of (7). In that case, the best one can hope for is that the system trajectories $\boldsymbol{q}(t)$ are ultimately bounded [26]. Consequently, the task for F reads as to converge into a ball $\mathcal{B}(\boldsymbol{r_d}, \epsilon_r)$ of radius $\epsilon_r > 0$ around a desired position $\boldsymbol{r_d} \in \mathcal{M}$.

1) Ultimate boundedness of the system trajectories into a ball $\mathcal{B}(\boldsymbol{r_d}, \epsilon_r)$: Building upon previous work of ours [22], we propose a feedback control law yielding ultimate boundedness of the trajectories $\boldsymbol{q}(t)$ of F into a ball around a desired position $\boldsymbol{r_d} \in \mathcal{M}$; to this end, we use a suitably defined *dipolar* vector field as a feedback motion plan [27] for F.

In principle, a dipolar vector field $\mathbf{F} : \mathbb{R}^2 \to \mathbb{R}^2$ has integral lines that all lead to the origin $(0, 0)$ of a global coordinate frame $\mathcal{G}'$ in $\mathbb{R}^2$, is non-vanishing everywhere in $\mathbb{R}^2$ except for the origin, and is analytically given as:

$$\mathbf{F}(\boldsymbol{\eta}) = \lambda(\boldsymbol{p}^{\top}\boldsymbol{\eta})\boldsymbol{\eta} - \boldsymbol{p}(\boldsymbol{\eta}^{\top}\boldsymbol{\eta}), \tag{10}$$

where $\lambda \geq 2$, $\boldsymbol{p} \in \mathbb{R}^2$ and $\boldsymbol{\eta} = \begin{bmatrix} \eta_x & \eta_y \end{bmatrix}^{\top}$ the position vector w.r.t. $\mathcal{G}'$. Its characteristic property is that all integral lines converge to the origin $(0, 0)$ parallel to the axis the vector $\boldsymbol{p}$ lies on, see also Fig. 2. Consequently, picking a vector $\boldsymbol{p} = \begin{bmatrix} p_x & p_y \end{bmatrix}^{\top}$ such that its orientation $\varphi_p \triangleq \mathrm{atan2}(p_y, p_x)$ w.r.t. $\mathcal{G}'$ coincides with a desired orientation η_{θ_d}, has the effect of reducing the orientation control for a unicycle vehicle into forcing it to align with the integral lines of the dipolar vector field while flowing towards the origin $(0, 0)$. If the vector $\boldsymbol{p}$ is assigned on a desired position $\boldsymbol{\eta_d} = \begin{bmatrix} \eta_{x_d} & \eta_{y_d} \end{bmatrix}^{\top}$, then one gets a dipolar vector field whose integral lines converge to $\boldsymbol{\eta_d}$ having by construction the desired orientation $\varphi_p \triangleq \eta_{\theta_d}$ there.

In order to get the analytic expression of a vector field $\mathbf{F}$ with the desired convergence properties w.r.t. a configuration $\boldsymbol{q_d} \in \mathcal{M}$ in the leader frame $\mathcal{L}$, take $\boldsymbol{p} = \begin{bmatrix} p_x & p_y \end{bmatrix}^{\top}$ such that $\varphi_p = \mathrm{atan2}(p_y, p_x) \triangleq \theta_d$ and substitute $\boldsymbol{\eta}$ with $\boldsymbol{r_1} \triangleq \boldsymbol{r} - \boldsymbol{r_d}$ in (10), where $\boldsymbol{r_1} = \begin{bmatrix} x_1 & y_1 \end{bmatrix}^{\top}$. The components F_x, F_y of the vector field $\mathbf{F}$ along the unit directions $\{\frac{\partial}{\partial x}, \frac{\partial}{\partial y}\}$ read:

$$\mathrm{F}_x = 2p_x {x_1}^2 - p_x {y_1}^2 + 3p_y x_1 y_1, \tag{11a}$$

$$\mathrm{F}_y = 2p_y {y_1}^2 - p_y {x_1}^2 + 3p_x x_1 y_1. \tag{11b}$$

Having the vector field (11) at hand, we state the following theorem regarding on the position trajectories $\boldsymbol{r}(t)$ of F:

Theorem 1: The position trajectories $\boldsymbol{r}(t) = \begin{bmatrix} x(t) & y(t) \end{bmatrix}^{\top}$ of the perturbed system (7) enter and remain into a ball $\mathcal{B}(\boldsymbol{r_d}, \epsilon_r)$ around a desired position $\boldsymbol{r_d} \in \mathcal{M}$, under the control law $\boldsymbol{v_F} = \begin{bmatrix} u_{\mathrm{F}} & w_{\mathrm{F}} \end{bmatrix}^{\top}$ where:

$$u_{\mathrm{F}} = -k_1 \,\mathrm{sgn}\left(\boldsymbol{r_1}^{\top} \begin{bmatrix} \cos\beta \\ \sin\beta \end{bmatrix}\right) \|\boldsymbol{r_1}\| - \mathrm{sgn}(\boldsymbol{p}^{\top}\boldsymbol{r_1}) u_{\mathrm{L}}^{\star}, \tag{12a}$$

$$w_{\mathrm{F}} = -k_2(\beta - \varphi) + \dot{\varphi}, \tag{12b}$$

$k_1, k_2 > 0$, $\varphi \triangleq \mathrm{atan2}(\mathrm{F}_y, \mathrm{F}_x)$ is the orientation of the vector field (11) at (x, y), $u_{\mathrm{L}}^{\star}$ is the upper bound of the linear velocity of L and $\epsilon_r > \frac{|w_{\mathrm{L}}|}{\sqrt{k_1 k_2}}$. The proof is given in the Appendix A.

Remark 2: A conservative, yet safe (worst-case) ϵ_r can be taken for the bound $w_{\mathrm{L}}^{\star}$ of the angular velocity of L. Note also that as $w_{\mathrm{L}} \to 0$, then $\epsilon_r \to 0$ as well.

2) Maintaining visibility: The necessary and sufficient conditions ensuring that system trajectories $\boldsymbol{q}(t)$ never escape a set of state constraints K are given by Nagumo's Theorem [21], [28]. Briefly, the main idea is that on the boundary ∂K of the set K, the system vector field $\dot{\boldsymbol{q}} \in T_{\boldsymbol{q}}\mathcal{C}$, with $T_{\boldsymbol{q}}\mathcal{C}$ being the tangent space of the state space $\mathcal{C}$ at the point $\boldsymbol{q}$, should be tangent to K, for bringing the solution $\boldsymbol{q}(t)$ back in the interior of K.[2] Thus, for the visibility set K considered here, the k-th constraint (8) is always maintained if and only if:

$$\frac{dh_k}{dt} = \nabla h_k \, \dot{\boldsymbol{q}} \overset{(7)}{=} \nabla h_k \, (\boldsymbol{f}(\boldsymbol{q}, \boldsymbol{v_F}) + \boldsymbol{g}(\boldsymbol{q}, \boldsymbol{v_L})) < 0, \quad \forall \{\boldsymbol{q} \in \mathcal{C} \mid h_k(\boldsymbol{q}) = 0\}, \tag{13}$$

where $\nabla h_k \triangleq \begin{bmatrix} \frac{\partial h_k}{\partial x} & \frac{\partial h_k}{\partial y} & \frac{\partial h_k}{\partial \beta} \end{bmatrix}$ is the gradient of $h_k(\cdot)$, and $k \in \{1, 2\}$. To see why, note that (13) implies that the value of the constraint function $h_k(\cdot) : \mathbb{R}^3 \to \mathbb{R}$ is forced to decrease, which in turn implies that the constraint function $h_k(\cdot)$ remains negative, or equivalently, that the resulting trajectory $\boldsymbol{q}(t)$ is forced to lie in the interior of the visibility set K. The necessary and sufficient conditions for maintaining visibility when *both* constraints are active *at the same time* are written using the Jacobian matrix $\boldsymbol{J_h}(\boldsymbol{q})$ of the map $\boldsymbol{h} = (h_1(\cdot), h_2(\cdot)) : \mathbb{R}^3 \to \mathbb{R}^2$ as:

$$\boldsymbol{J_h}(\boldsymbol{q})\dot{\boldsymbol{q}} < \mathbf{0}, \text{ where } \boldsymbol{J_h}(\boldsymbol{q}) = \begin{bmatrix} \frac{\partial h_1}{\partial x} & \frac{\partial h_1}{\partial y} & \frac{\partial h_1}{\partial \beta} \\ \frac{\partial h_2}{\partial x} & \frac{\partial h_2}{\partial y} & \frac{\partial h_2}{\partial \beta} \end{bmatrix}. \tag{14}$$

At this point, note that while the control law (12) does force F to converge into a ball around a desired position $\boldsymbol{r_d} \in \mathcal{M}$ — which by definition belongs to the visibility set K — it does not necessarily guarantee that the trajectories $\boldsymbol{q}(t)$ do always belong to the visibility set K. In other words, the resulting paths for F as it moves towards $\boldsymbol{q_d}$ may be such that L lies

[2] This tangency condition is realized via the concept of contingent cone $T_K(x)$ to a set K defined by inequality constraints [21], [29].

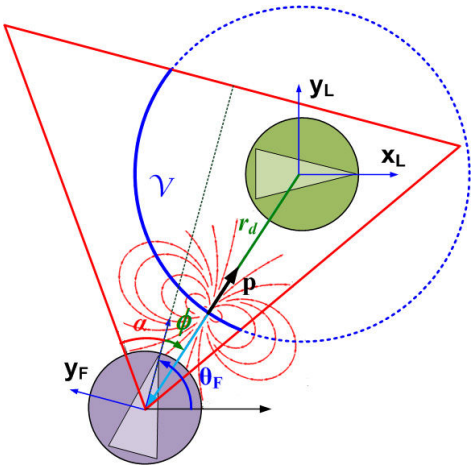

Fig. 2. Determining the vector $\boldsymbol{p}$ and the desired position $\boldsymbol{r_d}$ on $\mathbb{R}^2$

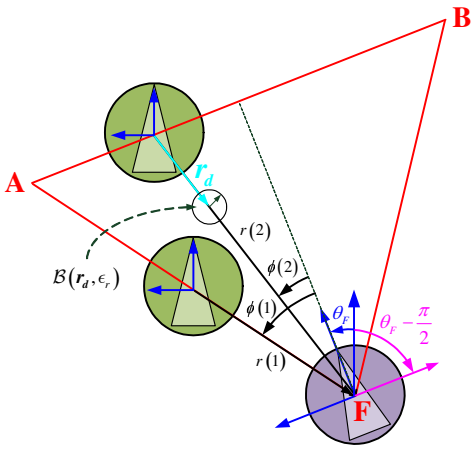

Fig. 3. In an obstacle-free environment, the viability constraints are active on the boundary of the cone of view (visibility at stake)

out of the visibility cone during some finite time intervals. For the problem setup and control design considered here, this primarily depends on the choice of the desired configuration $\boldsymbol{q_d} \in \mathcal{M}$, which in turn dictates the choice for the vector $\boldsymbol{p} \in \mathbb{R}^2$ in the definition of the vector field (11), i.e. dictates the reference orientation $\varphi(t)$ that F has to track via (12b).

In this respect, note that not all possible desired positions $\boldsymbol{r_d} \in \mathcal{M}$ for F belong to its cone-of-view at each time instant t. For instance, see Fig. 2 and assume that $t = 0$: the desired positions $\boldsymbol{r_d} \in \mathbb{R}^2$ belong to the circle $c = \{\boldsymbol{r} \in \mathbb{R}^2 \mid x^2 + y^2 = {r_d}^2\}$, centered at L; however, only the positions on the arc $\mathcal{V}$ shown in bold belong to the cone-of-view of F. Thus, one needs to pick some $\boldsymbol{r_d} \in \mathcal{V}$, which furthermore guarantees that visibility is always maintained.

A sufficient option is to choose the position $\boldsymbol{r_d} \in \mathcal{V}$ which lies on the line that connects the two robots. To see why, let us illustrate the necessary and sufficient visibility conditions (14) for the boundary configurations of the system shown in Fig. 3. The first visibility constraint is active when $h_1(\boldsymbol{q}) = 0 \Leftrightarrow \phi = \pm\alpha$; in this case, L lies on either the side AF, or the side BF of the cone-of-view. The second visibility constraint is active when $h_2(\boldsymbol{q}) = 0 \Leftrightarrow r = L_s \frac{\cos\alpha}{\cos\phi}$; in this case, L lies on the side AB. Worst case, the visibility constraints are both active

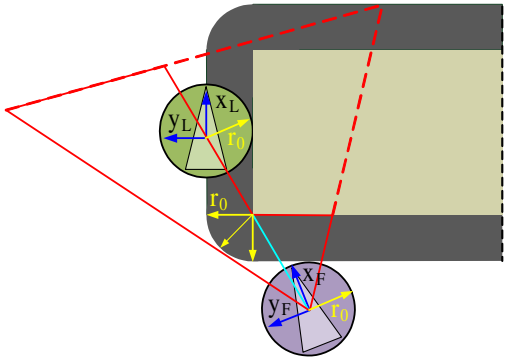

Fig. 4. In an obstacle environment, viability constraints are active on the boundary of the cone-of-view (visibility at stake) and on the boundary of the inflated obstacles (safety due to collisions at stake)

when L lies on either point A or point B. Then, visibility is maintained under the proposed control law (12) as long as the condition (14) holds. The analytical expression of the visibility conditions and a sufficient tuning of the control gains k_1, k_2 so that these conditions always hold, are given in Appendix B. With this at hand, we may now state the following theorem.

Theorem 2: The control law (12) with the control gains k_1, k_2 satisfying (23), (24), guarantees that the follower F:

- converges and remains into the ball $\mathcal{B}(\boldsymbol{r_d}, \epsilon_r)$,
- maintains visibility w.r.t. the leader L, and
- avoids collision with L.

Proof: The first two arguments were proved in Appendix A and Appendix B, respectively. For the third argument, let us consider the Lyapunov function $V_1 = \frac{1}{2}({x_1}^2 + {y_1}^2)$ encoding the squared distance between F and its goal position $\boldsymbol{r_d}$, and recall from the analysis in Appendix B that its time derivative $\dot{V}_1$ is negative out of the ball $\mathcal{B}(\boldsymbol{r_d}, \epsilon_r)$. This implies that the distance $\|\boldsymbol{r_1}\|$ of F to its goal $\boldsymbol{r_d} \in \mathcal{V}$ is always forced to decrease, until its value becomes lower than ϵ_r. Furthermore, by definition the goal position $\boldsymbol{r_d}$ for F is always picked to lie between the two robots, see Fig. 2. Let us assume that for some initial configuration $\boldsymbol{q_0} \in K$, the proposed control strategy forces F to collide with L; then, this implies that the distance $\|\boldsymbol{r_1}\|$ should increase, which is inconsistent for the system trajectories under (12). Therefore, inter-vehicle collision avoidance is always guaranteed. ■

IV. Motion Planning in Obstacle Environments

The L – F formation is assumed to move in a structured workspace $\mathcal{W} \subset \mathbb{R}^2$ with known obstacles, e.g. in an indoor corridor environment. For ensuring the safe and reliable motion of the robots one should take into account that:

1) obstacles may obstruct visibility (Fig. 4), and therefore if L is not visible to F, then sensing is not effective,
2) the trajectories $\boldsymbol{q_L}(t)$, $\boldsymbol{q_F}(t)$ should be collision-free.

The robots are represented as circular disks of radius r_0. This radius is added to the obstacles as shown in Fig. 4. Thus, the dark grey region around obstacles reduces the free space of the robots, while it does not affect visibility; F can still detect L through this region, but both F, L should not enter into it.

A. Motion Coordination in a Corridor Environment

Controlling F via (12) essentially yields the desired formation shape along with guaranteed visibility maintenance. For the navigation of the formation through a corridor environment we further need a motion plan for L. To this end, we first decompose the free space into cells as described in Appendix C. We also assume that L is given a high-level discrete motion plan indicating the sequence of cells that it has to go through, in order to converge to a goal configuration.

With these at hand, we are now pursuing a control strategy for L such that its motion guarantees obstacle avoidance for *both* robots; recall that the motion of F already guarantees the maintenance of the formation shape and visibility with L.

1) Defining local feedback motion plans for L*:* Given the sequence of cells $i \in \{1, 2, \ldots, N_{cell}\}$ that L has to go through, the motion planning for L follows the spirit presented in [30]. More specifically, in each cell i we define a dipolar vector field $\mathbf{F}_{\mathrm{L}\,i}$ (10) which serves as a local feedback motion plan for L in the following sense: the integral curves of the vector field $\mathbf{F}_{\mathrm{L}\,i}$ in cell i point into the interior of the successor cell $i+1$ on the exit face of the cell i, and into the interior of the cell i on each one of the remaining faces (Fig. 5).

The difference compared to [30] is that here the vector fields defined in each cell i are dipolar and thus their integral curves converge by construction to the midpoint of the exit face of cell i. This is ensured by assigning the dipole moment vector $\boldsymbol{p}_{\mathrm{L}\,i}$ of the vector field $\mathbf{F}_{\mathrm{L}\,i}$ on the exit point of the cell i.

The feedback motion plan for L can then be defined as to orient with and flow along the integral curves of the vector field $\mathbf{F}_{\mathrm{L}\,i}$ in each cell i.

Lemma 1: Let us assume that, worst case, L initiates on the boundary of a cell i, with orientation pointing into the interior of the cell. Then L performs collision-free motion throughout the successive cells $i, i+1, \ldots$, under the control inputs:

$$u_{\mathrm{L}} = \text{const} \leq u_{\mathrm{L}}^{\star}, \tag{15a}$$

$$w_{\mathrm{L}} = -k_{\mathrm{L}}(\theta_{\mathrm{L}} - \varphi_{\mathrm{L}\,i}) + \dot{\varphi}_{\mathrm{L}\,i}, \tag{15b}$$

where $\varphi_{\mathrm{L}\,i}$ is the orientation of the vector field $\mathbf{F}_{\mathrm{L}\,i}$ in cell i, and $k_{\mathrm{L}} > 0$.

Proof: Since each vector field $\mathbf{F}_{\mathrm{L}\,i}$ by definition points into the interior of the free space, it follows that obstacle avoidance for L is ensured. ■

Remark 3: The motion and resulting trajectories $\boldsymbol{q}_{\mathbf{L}}(t)$ of L *essentially dictate the desired position trajectories $\boldsymbol{r}_{\boldsymbol{d}}(t) \in \mathcal{V}$ (see Fig. 2) that* F *has to track at each* t*. Clearly, $\boldsymbol{r}_{\boldsymbol{d}}(t)$ should always lie in the free space.* To see if this is always the case, let us first consider the motion of the formation when both robots lie in the same cell i.

Lemma 2: Let us assume that L, F start in the *same* cell i, at some initial distance $r > r_d$ and so that the visibility constraints are not violated. We furthermore assume that when initiating on the boundary of the cell, the orientations of L, F point into the interior of the cell. Then under the control laws (15), (12) the motion of the $\mathrm{L}-\mathrm{F}$ formation in cell i remains collision free.

Proof: Worst case, both robots start on the boundary of the free space so that at least one of the visibility constraints is active. Then out of Lemma 1 one has that L moves into the interior of cell i. Furthermore, out of Theorem 2 one has that the inter-agent distance r decreases, implying thus that F is forced to move into the interior of the cell i. Thus, both robots avoid static obstacles. Inter-robot collision avoidance is also guaranteed out of Theorem 2. Consequently, the motion of the $\mathrm{L}-\mathrm{F}$ formation in cell i is collision-free. ■

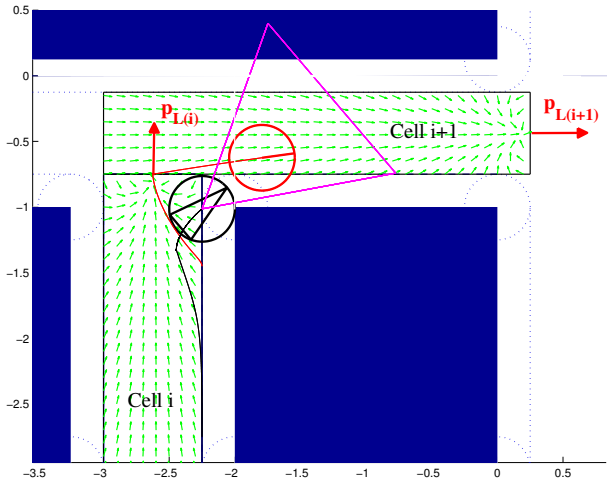

Fig. 5. L moves through the successive cells i, $i+1$ under (15), tracking the vector fields shown in the free space. The resulting trajectory $\boldsymbol{q}_{\mathbf{L}}(t)$ will likely force F to eventually collide with obstacles. Thus, L, F should move with minimum turning radii R_{L}, R_{F} around corners.

Let us now consider the transition when L enters cell $i+1$ while F is still in cell i. In this case, it is likely that the trajectory $\boldsymbol{q}_{\mathbf{L}}(t)$ will force the desired position $\boldsymbol{r}_{\boldsymbol{d}}$ to eventually enter the obstacle space. To see how, consider Fig. 5: L is forced to track the vector field in cell $i+1$ after exiting cell i and thus moves in the free space but very close to the obstacle, forcing F to eventually collide with the obstacle.

2) Considering the formation as a Tractor-Trailer system: This remark essentially implies that L should move with a minimum turning radius R_{L} when entering into cell $i+1$, so that the trajectories $\boldsymbol{q}_{\mathbf{F}}(t)$ do not enter the obstacle space. A sufficient way to ensure this is to think of the $\mathrm{L}-\mathrm{F}$ formation as a tractor (L) pulling a trailer (F) with axle-to-axle hitching of length r_d [23] when turning around corners.[3]

Lemma 3: If L starts moving along a circle of center C and radius R_{L}, then F will move on a circle of the same center C and radius $R_{\mathrm{F}} = \sqrt{{R_{\mathrm{L}}}^2 - {r_d}^2}$.

Proof: It trivially follows out of the kinematics of a tractor-trailer system, see [23]. ■

Thus, if R_{L}, R_{F} can be picked so that they dictate collision-free paths for the tractor-trailer system, then it naturally follows that the trajectories of both L and F are collision-free.

Theorem 3: Assume that L is at the midpoint M_i of a cell i—driven there by (15)— and starts moving in cell $i+1$ along a circle of radius R_{L}, whereas F is in cell i, at a distance r_d

[3]Equivalently, the formation can be kinematically seen as a front-wheel driven car, where $\beta = \theta_{\mathrm{F}} - \theta_{\mathrm{L}}$ is the steering angle and r_d is the wheelbase. Note that this assumption is valid since, after F has converged into $\mathcal{B}(\boldsymbol{r}_{\boldsymbol{d}}, \epsilon_r)$ where $\epsilon_r \to 0$, it is guaranteed to remain there and also to keep a relative angle $\phi \to 0$ w.r.t. L.

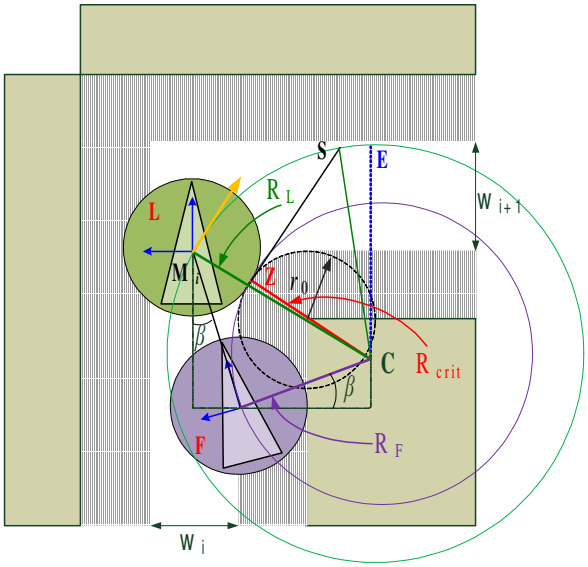

Fig. 6. After exiting cell i, L should move in cell $i+1$ along a circle of radius $R_{\rm L}$ that satisfies (16).

w.r.t. L. If the turning radius $R_{\rm L}$ satisfies:

$$\sqrt{{r_d}^2+{R_{\rm F_w}}^2} \le R_{\rm L} \le w_{i+1}+R_{\rm F_w}\frac{w_i}{2r_d}+\sqrt{{r_d}^2-\frac{{w_i}^2}{4}}, \quad (16)$$

where w_i, w_{i+1} are the lengths of the exit faces of the cells i, $i+1$, respectively, r_0 is the radius of the robots and

$$R_{\rm F_w}=\frac{\left(\frac{r_0}{2}\sqrt{2}-r_0+\sqrt{{r_d}^2-\frac{{w_i}^2}{4}}\right)^2+\left(\frac{r_0}{2}\sqrt{2}-r_0\right)^2}{\frac{w_i}{r_d}\sqrt{{r_d}^2-\frac{{w_i}^2}{4}}+\frac{w_i r_0}{r_d}\left(\frac{\sqrt{2}}{2}-1\right)-\frac{2r_0}{r_d}\sqrt{{r_d}^2-\frac{{w_i}^2}{4}}\left(\frac{\sqrt{2}}{2}-1\right)}, \quad (17)$$

then the trajectories $\boldsymbol{q}_{\mathbf{L}}(t)$, $\boldsymbol{q}_{\mathbf{F}}(t)$ are collision-free.

Proof: Let us consider Fig. 6 and denote with $t^\star$ the time instant when L is at the midpoint M_i of the cell i. L moves in cell $i+1$ along a circle of center C and radius $R_{\rm L}$. Since F behaves kinematically as a trailer, one has out of Lemma 3 that it moves along a circle of the same center C and radius $R_{\rm F}=\sqrt{{R_{\rm L}}^2-{r_d}^2}$.

In the depicted scenario, $R_{\rm F}$ is drawn to actually be the smallest critical value $R_{\rm F,cr}$ for which the trajectories $\boldsymbol{q}_{\rm F}(t)$ remain collision-free. Furthermore, this corresponds to the worst case, with F starting/being on the boundary of the free space.[4] The position coordinates of F w.r.t. a coordinate frame $\mathcal{L}^\star$ attached on the midpoint M_i of the exit face of cell i are:

$$x_{\rm F_w}=-\sqrt{{r_d}^2-\frac{{w_i}^2}{4}}, \quad y_{\rm F_w}=-\frac{w_i}{2},$$
$$\cos(\beta_{\rm w})=\frac{\sqrt{{r_d}^2-\frac{{w_i}^2}{4}}}{r_d}, \quad \sin(\beta_{\rm w})=\frac{w_i}{2r_d}.$$

Furthermore, the center of rotation C is constant and its position w.r.t. $\mathcal{L}^\star$ is:

$$x_C=x_{\rm F_w}+R_{\rm F}\sin(\beta_{\rm w}),\ y_C=y_{\rm F_w}-R_{\rm F}\cos(\beta_{\rm w}),$$

[4]Clearly, this $R_{\rm F,cr}$ corresponds to L making a right turn. Similarly one can treat the case for a left turn.

whereas the coordinates of the critical point Z w.r.t. $\mathcal{L}^\star$ are:

$$x_{\rm Z}=\frac{r_0\sqrt{2}}{2}-r_0,\ y_{\rm Z}=-\frac{w_i}{2}+\frac{r_0\sqrt{2}}{2}-r_0. \text{ Thus,}$$
$$R_{\rm F,cr}=\sqrt{(x_C-x_{\rm Z})^2+(y_C-y_{\rm Z})^2}. \quad (18)$$

Substituting the expressions above into (18) and after some algebra one can verify that the analytical expression for the worst-case safe turning radius $R_{\rm F_w}=R_{\rm F_{cr}}$ is given by (17).[5] It follows that if L moves into cell $i+1$ with turning radius $R_{\rm L}\ge\sqrt{{r_d}^2+{R_{\rm F_w}}^2}$, then the trajectories of F in cells i, $i+1$ are collision-free. This proves the left inequality in condition (16). The right inequality is trivially derived out of the geometry of Fig. 6 by requiring $R_{\rm L}\le CE$, in order to ensure that the motion of L along the arc M_iE in the cell $i+1$ is collision-free as well. In summary, picking a turning radius $R_{\rm L}$ satisfying the condition (16) guarantees that the transition of the L − F formation between cells i and $i+1$ is collision-free. ■

Remark 4: The condition (16) is rather conservative, in the sense that $R_{\rm F_w}$ is computed for the *worst-case* scenario, *since we assumed that* L *has no information on the position of* F. Thus, given r_d, r_0 and the cell decomposition, it is easy to a priori check whether a safe $R_{\rm L}$ exists for each one of the transitions between cells that are realized as turning around corners. Given that a safe $R_{\rm L}$ exists, the motion of the L − F formation is dictated by the following control strategy:

1) Both robots initiate and move in the same cell i, according to the assumptions and control laws in Lemma 2.
2) L reaches a ball of arbitrarily small radius around the midpoint M_i of the exit face of cell i: Then, L (i) orients with the tangent vector to the radius CM_i, whose direction is computed as: $\lambda_{\rm T}=-\frac{x_C(t^\star)}{y_C(t^\star)}=-\frac{x_{\rm F_w}+R_{\rm F_w}\sin(\beta_{\rm w})}{y_{\rm F_w}-R_{\rm F_w}\cos(\beta_{\rm w})}$, and (ii) moves into cell $i+1$ with linear velocity given by (15a) and angular velocity $w_{\rm L}^{\rm T}=\text{sign}(w_{\rm L})\frac{u_{\rm L}}{R_{\rm L}}$, where $w_{\rm L}$ is given by (15b). Then L travels arbitrarily close to the circle of radius C and radius $R_{\rm L}$.
3) L reaches a ball of arbitrarily small radius around the point E (Fig. 6). Then F has already entered safely in the cell $i+1$.[6] The angular velocity control for L switches to (15b) and L tracks the vector field in cell $i+1$ on its way to the exit face of this cell.
4) L reaches a ball of arbitrarily small radius around the midpoint of the exit face of cell $i+1$. Then L switches to the control strategy described in Step (2), and so on.

Remark 5: The worst-case computation of safe $R_{\rm L}$, $R_{\rm F}$ does not need to be done for L exiting at the midpoint M_i of the exit face of cell i. One may tune the proximity of the resulting trajectories $\boldsymbol{q}_{\mathbf{L}}(t)$, $\boldsymbol{q}_{\mathbf{F}}(t)$ to the obstacles by sliding the exit point of L along the exit face of cell i. This is further illustrated in the extension discussed below.

[5]Not surprisingly, the critical turning radius for F depends on the radius r_0 of the robots, the distance r_d between them and the width w_i of cell i. Furthermore, one may easily verify that (17) is always well-defined (positive), since the denominator is positive for the worst case, i.e. for $w_i=r_0$ and $r_d=2r_0$.

[6]Actually F enters safely in the cell $i+1$ when L lies on the point S.

B. Motion Coordination for $N > 2$ robots

The tractor-pulling-trailers paradigm can be used to extend the proposed motion planning and coordination control in the case of $\mathrm{N} > 2$ robots that move in a chain formation of one global leader L and $\mathrm{N}-1$ followers F_j, $j \in \{1, \ldots, \mathrm{N}-1\}$. In such formation, F_k serves as a local leader to $\mathrm{F}_{(k+1)}$, so that $\mathrm{F}_{(k+1)}$ is localized w.r.t. F_k, $k \in \{1, \ldots, \mathrm{N}-2\}$.

The feedback motion plan for L follows the idea presented above: given a decomposition of convex cells and a high-level discrete motion plan, the motion of L in a cell i is dictated by a local dipolar vector field $\mathbf{F}_{\mathrm{L}\,i}$, defined so that its integral curves converge to *some* point N_i on the exit face of cell i; the determination of this exit point is given later on.

To ensure the collision-free transition of *all* followers F_j from cell i to cell $i+1$, one may pick a turning radius R_{L} for L (tractor) such that the trajectories of the *last* follower (trailer) $\mathrm{F}_{(\mathrm{N}-1)}$ remain collision-free. Let us denote the worst-case safe turning radius for $\mathrm{F}_{(\mathrm{N}-1)}$ with $R_{\mathrm{F_w}}$; this corresponds to $\mathrm{F}_{(\mathrm{N}-1)}$ being on the boundary of cell i at the time instant that $\mathrm{F}_{(\mathrm{N}-2)}$ exits cell i.

Given that under (12) each follower F_k acts as a local leader (i.e. tractor) to $\mathrm{F}_{(k+1)}$, it follows out of the kinematics of a tractor-trailer system [23] that the turning radii R_{F_k} of each follower F_k, $k \in \{1, \ldots, \mathrm{N}-2\}$ satisfy:

$$R_{\mathrm{F}_{(\mathrm{N}-2)}}{}^2 = R_{\mathrm{F_w}}{}^2 + r_d{}^2, \tag{19a}$$
$$R_{\mathrm{F}_{(\mathrm{N}-3)}}{}^2 = R_{\mathrm{F}_{(\mathrm{N}-2)}}{}^2 + r_d{}^2, \tag{19b}$$
$$\vdots$$
$$R_{\mathrm{F}_2}{}^2 = R_{\mathrm{F}_3}{}^2 + r_d{}^2, \tag{19c}$$
$$R_{\mathrm{F}_1}{}^2 = R_{\mathrm{F}_2}{}^2 + r_d{}^2, \tag{19d}$$

and similarly the turning radius of L is given as $R_{\mathrm{L}}{}^2 = R_{\mathrm{F}_1}{}^2 + r_d{}^2$. Substituting (19) into this expression yields:

$$R_{\mathrm{L}}{}^2 = \left(R_{\mathrm{F_w}}{}^2 + (\mathrm{N}-2) r_d{}^2\right) + r_d{}^2 = R_{\mathrm{F_w}}{}^2 + (\mathrm{N}-1) r_d{}^2 \tag{20}$$

with $R_{\mathrm{F_w}}$ computed for $\mathrm{F}_{(\mathrm{N}-1)}$ being on the boundary of the cell i at the time instant when $\mathrm{F}_{(\mathrm{N}-2)}$ exits cell i. The exit point for $\mathrm{F}_{(\mathrm{N}-2)}$ is picked by the designer and it does not need to coincide with the midpoint of the exit face. Following the pattern in Theorem 3, one may compute the position coordinates of the last follower $\mathrm{F}_{\mathrm{N}-1}$, the center C and the critical point Z w.r.t. a global frame attached to this exit point, and derive the worst-case $R_{\mathrm{F_w}}$ out of (18), which reads:

$$R_{\mathrm{F_w}} = \frac{r_d \left[\left(r_0 - \frac{r_0}{\sqrt{2}} + x_{\mathrm{F_w}} \right)^2 + \left(r_0 - \frac{r_0}{\sqrt{2}} \right)^2 \right]}{2 \left(y_{\mathrm{F_w}} - x_{\mathrm{F_w}} \right) \left(r_0 - \frac{r_0}{\sqrt{2}} \right) + 2\, y_{\mathrm{F_w}}\, x_{\mathrm{F_w}}}. \tag{21}$$

The derivation of $R_{\mathrm{F_w}}$ is straightforward and omitted here in the interest of space. Having (20), (21) at hand, it is now easy to compute the coordinates of the exit point N_i for L on the exit face of i. Consider Fig. 7, depicting the worst-case exit scenario for $\mathrm{F}_{(\mathrm{N}-2)}$, $\mathrm{F}_{(\mathrm{N}-1)}$. At this time instant, L already lies in cell $i+1$ traveling along the circle of center C and radius R_{L}. The coordinates of the exit point N_i for L are computed by applying the law of cosines for the triangle $(N_i\, \mathrm{F}_{(\mathrm{N}-2)}\, C)$ to compute the length of the side $(N_i\, \mathrm{F}_{(\mathrm{N}-2)})$. L should move along the safe R_{L} until reaching the safe point S, so that F enters safely in cell $i+1$, i.e. so that F reaches the critical point Z. The coordinates of S are a priori computed using (19), see Fig. 7 the case of $N = 4$ agents. Clearly, the coordinates of S should lie in the interior of cell $i+1$.

Therefore, the control strategy for L in the case of $\mathrm{N} > 2$ agents reads: While in cell i, L tracks a dipolar vector field (10) defined with its dipole moment vector $\boldsymbol{p}_{\mathrm{L}\,i}$ assigned on the exit point N_i. For the transition from cell i to cell $i+1$, L is controlled as described in the previous section with R_{L} given by (20) until reaching the point S, while each F_j is controlled via (12). The turning radius R_{L} (20) ensures the (worst-case) turning radius $R_{\mathrm{F_w}}$ for the last follower $\mathrm{F}_{(\mathrm{N}-1)}$ is safe, i.e. that the transition of the chain formation between cells i, $i+1$ is collision-free.

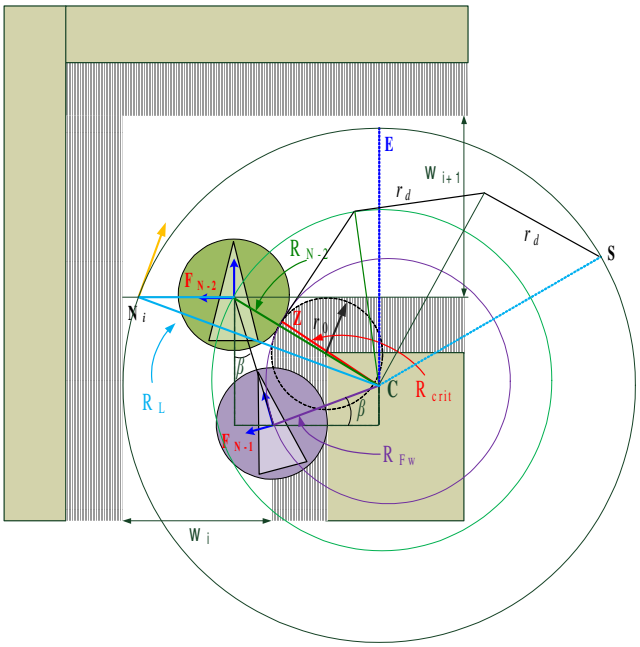

Fig. 7. Computing the exit point of L on the exit face of cell i when $\mathrm{N} > 2$.

C. Motion Coordination in Complex Polygonal Environments

The proposed control strategy for L is not restricted to rectangular cells, but can rather be applied in general polygonal obstacle environments. Given a cell decomposition of convex polygonal cells (Appendix C) L may track a local dipolar vector field in cell i, defined in the sense described above. The tractor-pulling-trailers paradigm can be used for the computation of turning radii R_{L}, $R_{\mathrm{F_w}}$ that realize the worst-case, yet safe, transition from cell i to cell $i+1$. This becomes evident in Fig. 6, 7, 13: the turning radii around corners are essentially computed by embedding circles (i.e. paths) consistent with the tractor-trailer kinematics. Thus, given that cell decomposition is known, one can compute the worst-case safe R_{L}, $R_{\mathrm{F_w}}$ for any transition between successive cells.

V. Simulation Results

The efficacy of the proposed motion planning and coordination strategy is evaluated through computer simulations.

A decomposition of the free space into polygonal cells (see Appendix C) and a high-level discrete motion plan is given to L. All robots initiate so the corresponding visibility constraints are satisfied, while initial conditions with the robots being in different cells should be avoided, in the sense that they may by definition violate the safe curvatures around corners.

The scenario depicted in Fig. 9 involves $\mathrm{N} = 4$ robots, one leader L (in red) and three followers F_j, $j \in \{1, 2, 3\}$, and demonstrates the collision-free motion of the formation during the transition between cells i and $i+1$. All robots initiate in cell i, positioned on the boundaries of the obstacles. The cones-of-view are not illustrated, to avoid getting the figure congested. F_1 (resp. F_2, F_3) is localized w.r.t. to L (resp. F_1, F_2), yet is neither aware of its motion plan, nor of its velocities at each time t. The system parameters are picked as: $r_0 = 0.25$ m, $\alpha = 30$ deg, $r_d = 0.6$ m, $w_i = 0.75$ m, $w_{i+1} = 0.625$ m.

L starts moving with constant linear velocity $u_{\mathrm{L}} \leq u_{\mathrm{L}}^{\star}$ and tracks a dipolar vector field in cell i on its way to the point N_i on the exit face of i, which is marked in Fig. 9(o). The position coordinates of N_i are dictated by the pre-computed safe R_{L}, $R_{\mathrm{F_w}}$ (Section IV-B). Here the worst-case safe turning radius for the last follower F_3 is derived out of (21) equal to $R_{\mathrm{F_w}} = 0.451509$ m. Thus out of (20) one has $R_{\mathrm{L}} = 1.13308$ m. At the same time, F_1 (resp. F_2, F_3) moves under the control law (12) and converge into a neighborhood around the desired configuration w.r.t. L (resp F_1, F_2), yielding thus the chain formation.

When L reaches the exit face of cell i, it is forced to follow a bounded curvature within cell $i+1$ to move around the corner under the angular velocity $w_{\mathrm{L}}^{\intercal} = \mathrm{sign}(w_{\mathrm{L}})\frac{u_{\mathrm{L}}}{R_{\mathrm{L}}}$, where w_{L} is the angular velocity (15b) dictated by the dipolar vector field in cell $i+1$. At the same time, the followers behave like trailers under their corresponding control laws (12), and thus start moving along circles of radii $R_{\mathrm{F}_j} > R_{\mathrm{F_w}}$ which are guaranteed to be collision-free (Section IV-B). As soon as L reaches the point S, it continues moving under the angular velocity w_{L} (15b) dictated by the vector field in cell $i+1$, until it reaches the exit face of the cell $i+1$, and so on. Fig. 9(o) demonstrates that the resulting paths for all agents are collision-free. Finally, Fig. 8 demonstrates the system response during the motion of the formation throughout a corridor environment under the cell decomposition described in Appendix C. The initial conditions are those depicted in Fig. 9, while the exit points N_i on the exit faces of cells i are marked with green and have been a priori computed as described in Section IV-B.

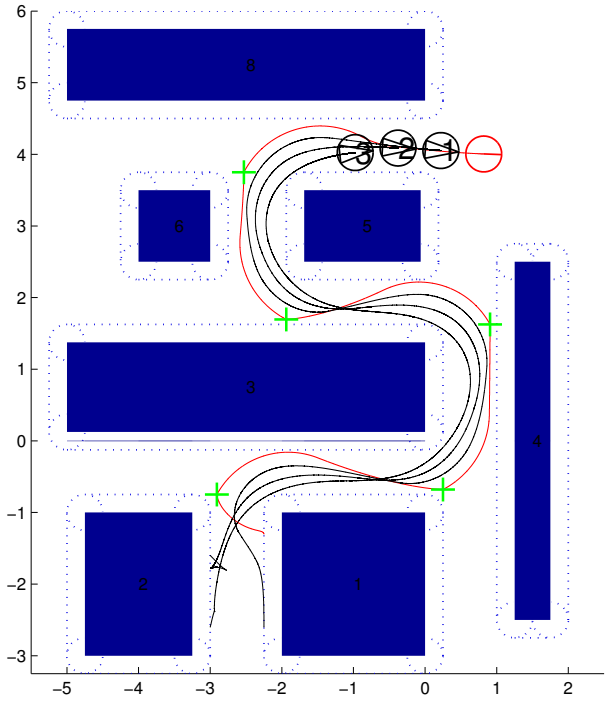

Fig. 8. The robots initiate on the boundary of the cell i, so that the second visibility constraint is additionally active for F_1.

VI. Discussion

This paper presented a motion coordination and control strategy for $\mathrm{L}-\mathrm{F}$ formations of nonholonomic vehicles, under visibility and communication constraints in known obstacle environments. Visibility constraints arise due to the limited vision-based sensing of the robots and define a visibility cone for each robot i.[7] A robot i is localized w.r.t. a robot j if and only if j belongs into the visibility cone of i. Thus, j and i can move as a $\mathrm{L}-\mathrm{F}$ pair if and only if j is always visible from i. Inter-vehicle collisions and avoidance of physical obstacles should also be ensured. For the guaranteed accomplishment of those multiple objectives, ideas from set-theoretic methods in control were combined with feedback motion planning via dipolar vector fields and the consideration of the formation as a tractor-trailer system, to the derivation of a hybrid control strategy. The proposed algorithms are decentralized, in the sense that they are dependent on local information only, which is online or a priori available to each robot, without the need for exchanging information.

It is worth noting that the computation of the safe turning radius for L is done for the worst-case scenario, i.e. for the last follower exiting cell i on the boundary of the obstacle. As thus, the consideration of the formation as a tractor-pulling-trailers system serves not only as one of the main contributions of this work, but also eliminates the need for communication among agents (i.e. the followers do not need to communicate their current positions to the leader for safely coordinating their motion, since the safe turning radii for the leader and the last follower are a priori computed for the worst-case condition). In this sense, this may be also seen as a robustness feature against communication failures, which may be relevant in other formation/communication topologies and similar multi-agent coordination problems in constrained environments, and is therefore an open direction for future investigation.

Our ongoing work and plans for future extensions are related to investigating switching control designs that may offer enhanced reliability and robustness in the case of malfunctioning, for instance against agent failures and measurement noise. As far as mechanical failures are concerned, let us note that the current approach does offer guarantees in terms of

[7]The assumption on the sensor footprint being an isosceles triangle is not restrictive, since the conditions (13) on maintaining visibility apply to any closed convex footprint, described by k inequalities $h_k(\cdot) \leq 0$.

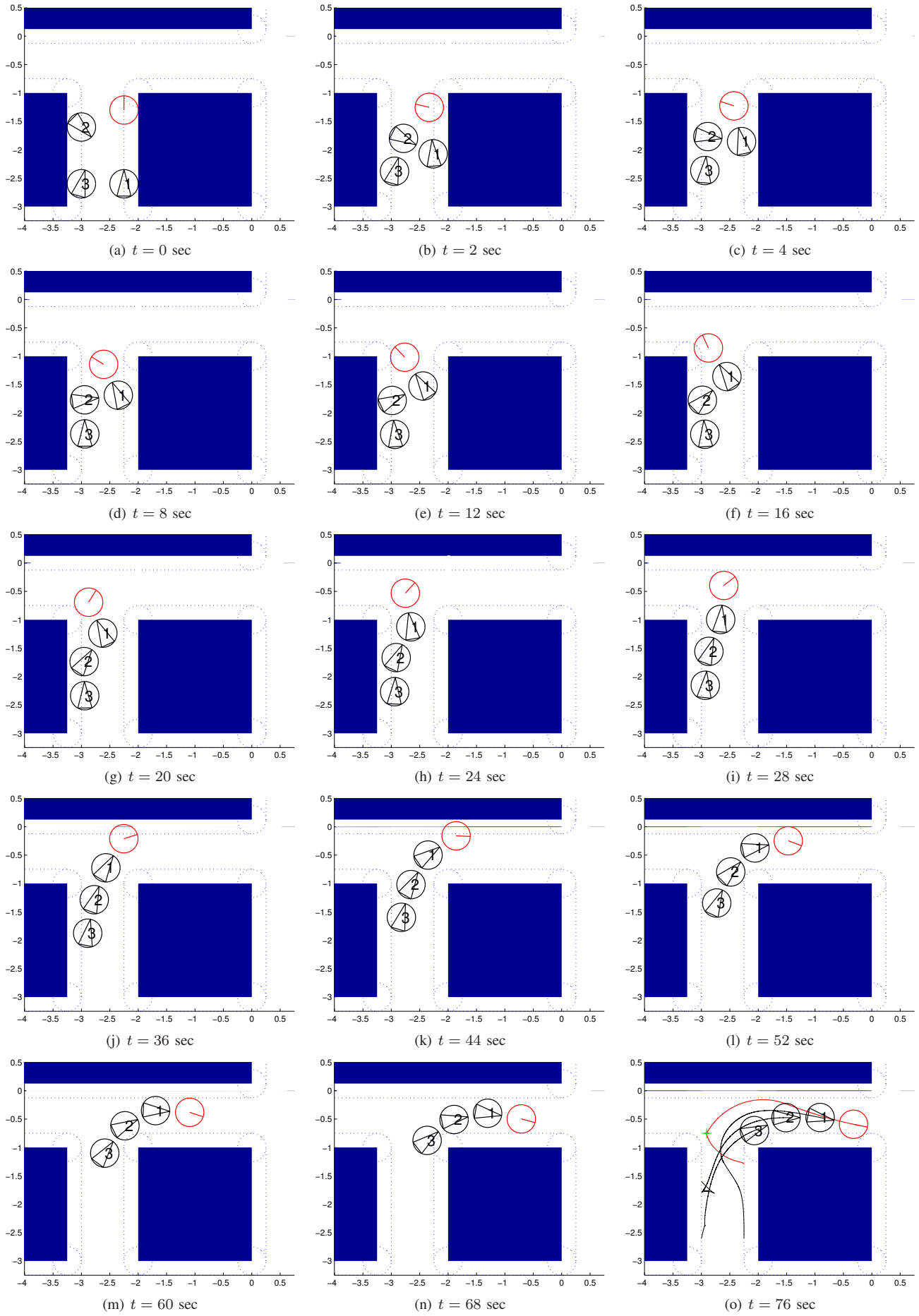

(a) $t = 0$ sec (b) $t = 2$ sec (c) $t = 4$ sec

(d) $t = 8$ sec (e) $t = 12$ sec (f) $t = 16$ sec

(g) $t = 20$ sec (h) $t = 24$ sec (i) $t = 28$ sec

(j) $t = 36$ sec (k) $t = 44$ sec (l) $t = 52$ sec

(m) $t = 60$ sec (n) $t = 68$ sec (o) $t = 76$ sec

Fig. 9. Four robots initiating in cell i move in (chain) formation using local information only.

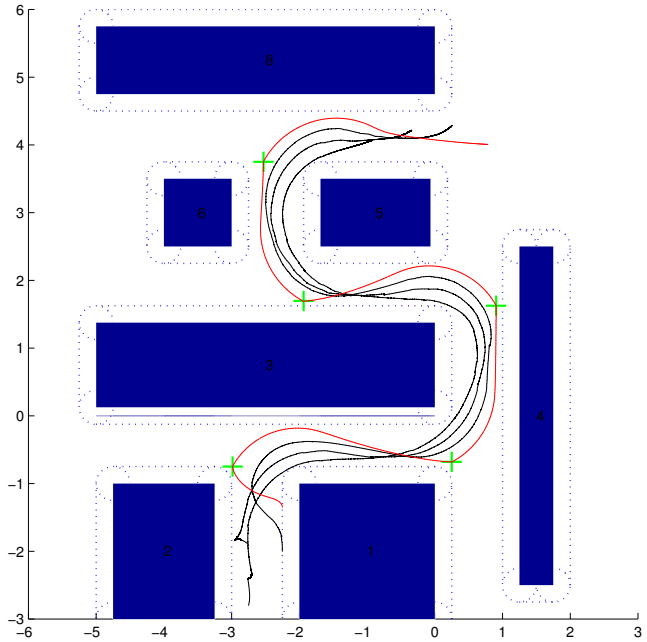

Fig. 10. The resulting paths under the effect of zero mean gaussian noise.

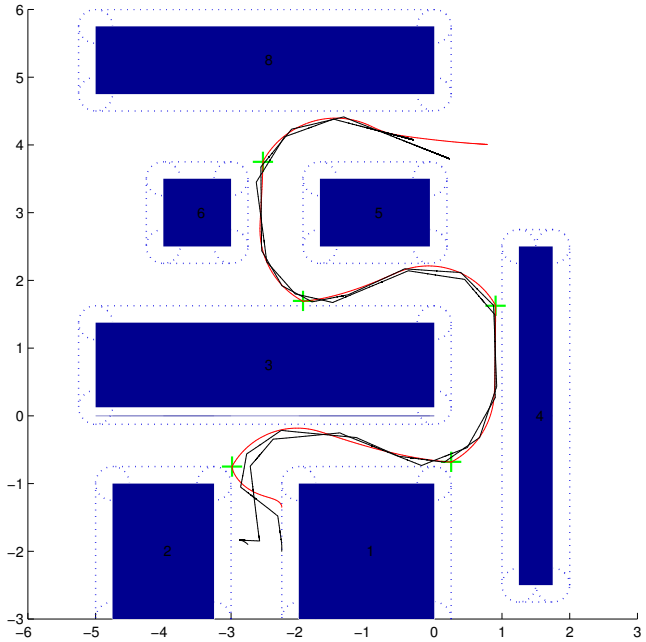

Fig. 11. The resulting paths under the effect of zero mean gaussian noise and a hysteresis technique on the orientation control.

avoiding collisions, since each agent is always guaranteed to keep a fixed distance w.r.t. the agent moving in front of it. Thus, if a robot i accidentally stops moving, then its follower $i+1$ will keep a fixed distance w.r.t. the robot i by remaining around its target point, forced there by proposed controllers. Of course, this implies that the formation will unavoidably break; for these reason, an interesting direction for further investigation is towards adding additional, "recovery control" modes into the existing hybrid system, which will become active in the case that an agent needs to pick a new (local) leader and coordinate its motion around a failed robot. Finally, the adoption of the nominal system so far, i.e. under the assumption of zero noise, is not restrictive in extending and generalizing the proposed control design, since the ideas and the mathematical framework can incorporate the effect of measurement noise and additive disturbances. Keeping in mind that the problem at hand involves wheeled robots operating in indoor environments, we ran some preliminary simulations with the position measurements of each robot corrupted by zero mean noise; this captures in spirit the observation noise expected in vision-based sensing and estimation, while the process noise in such environments for is typically not that great and thus was neglected. The simulations indicate that the current controller works well for relatively small estimation errors in position (of order $1-2\%$, see Fig. 10), while hysteresis-like techniques [31] on the orientation control offer enhanced robustness against larger position errors (of order $10-15\%$, see Fig. 11 a scenario with N $=$ 3 robots). The conditions which couple the admissible noise/disturbance characteristics with the safe turning radii, the environmental clearance and the robots' control gains require an extensive analysis which is out of the scope and the limits of the current paper, and is currently ongoing work.

REFERENCES

[1] J. P. Desai, J. P. Ostrowski, and V. Kumar, "Modeling and control of formations of nonholonomic mobile robots," *IEEE Trans. on Robotics and Automation*, vol. 17, no. 6, pp. 905–908, Dec. 2001.

[2] A. K. Das, R. Fierro, V. Kumar, J. P. Ostrowski, J. Spletzer, and C. J. Taylor, "A vision-based formation control framework," *IEEE Trans. on Robotics and Automation*, vol. 18, no. 5, pp. 813–825, Oct. 2002.

[3] N. Cowan, O. Shakernia, R. Vidal, and S. Sastry, "Vision-based follow-the-leader," in *Proc. of the 2003 IEEE/RSJ Int. Conf. on Intelligent Robots and Systems*, Las Vegas, Nevada, Oct. 2003, pp. 1796–1801.

[4] H. G. Tanner, G. J. Pappas, and V. Kumar, "Leader-to-Formation Stability," *IEEE Trans. on Robotics and Automation*, vol. 20, no. 3, pp. 443–455, Jun. 2004.

[5] G. L. Mariottini, F. Morbidi, D. Prattichizzo, G. J. Pappas, and K. Daniilidis, "Leader-follower formations: Uncalibrated vision-based localization and control," in *Proc. of the 2007 IEEE Int. Conf. on Robotics and Automation*, Roma, Italy, Apr. 2007, pp. 2403–2408.

[6] G. L. Mariottini, F. Morbidi, D. Prattichizzo, N. Vander Valk, G. Pappas, and K. Daniilidis, "Vision-based localization for leader-follower formation control," *IEEE Transactions on Robotics*, vol. 25, no. 6, pp. 1431–1438, Dec. 2009.

[7] O. A. Orqueda and R. Fierro, "Robust vision-based nonlinear formation control," in *Proc. of the 2006 American Control Conference*, Minneapolis, Minnesota, USA, Jun. 2006, pp. 1422–1427.

[8] H. Kannan, V. K. Chitrakaran, D. M. Dawson, and T. Burg, "Vision-based leader/follower tracking for nonholonomic mobile robots," in *Proc. of the 2007 American Control Conference*, New York City, USA, Jul. 2007, pp. 2159–2164.

[9] H. J. Min, A. Drenner, and N. Papanikolopoulos, "Vision-based leader-follower formations with limited information," in *Proc. of the 2009 IEEE Int. Conf. on Robotics and Automation*, Kobe, Japan, May 2009, pp. 351–356.

[10] G. Kantor and A. A. Rizzi, "Feedback control of underactuated systems via sequential composition: Visually guided control of a unicycle," in *Robotics Research*, P. Dario and R. Chatila, Eds. Springer Berlin Heidelberg, 2005, pp. 281–290.

[11] G. A. D. Lopes and D. E. Koditschek, "Visual servoing for nonholonomically constrained three degree of freedom kinematic systems," *The Int. Journal of Robotics Research*, vol. 26, no. 7, pp. 715–736, Jul. 2007.

[12] S. Bhattacharya, R. Murrieta-Cid, and S. Hutchinson, "Optimal paths for landmark-based navigation by differential-drive vehicles with field-of-view constraints," *IEEE Transactions on Robotics*, vol. 23, no. 1, pp. 47–59, Feb. 2007.

[13] P. Salaris, D. Fontanelli, L. Pallottino, and A. Bicchi, "Shortest paths for a robot with nonholonomic and field-of view constraints," *IEEE Transactions on Robotics*, vol. 26, no. 2, pp. 269–280, Apr. 2010.
[14] F. Morbidi, F. Bullo, and D. Prattichizzo, "Visibility maintenance via controlled invariance for leader-follower vehicle formations," *Automatica*, vol. 47, no. 5, pp. 1060–1067, May 2011.
[15] R. Murrieta-Cid, U. Ruiz, J. L. Marroquin, J.-P. Laumond, and S. Hutchinson, "Tracking an omnidirectional evader with a differential drive robot," *Autonomous Robots*, vol. 18, no. 4, pp. 345–366, Nov. 2011.
[16] U. Ruiz and R. Murrieta-Cid, "A homicidal differential drive robot," in *Proc. of the 2012 IEEE Int. Conf. on Robotics and Automation*, St. Paul, Minnesota, USA, May 2012, pp. 3218–3225.
[17] S. M. LaValle, H. H. González-Baños, C. Becker, and J.-C. Latombe, "Motion strategies for maintaining visibility of a moving target," in *Proc. of the 1997 IEEE Int. Conf. on Robotics and Automation*, Albuquerque, New Mexico, Apr. 1997, pp. 731–736.
[18] R. Murrieta-Cid, L. Munoz-Gomez, M. Alencastre-Miranda, A. Sarmiento, S. Kloder, S. Hutchinson, F. Lamiraux, and J. P. Laumond, "Maintaining visibility of a moving holonomic target at a fixed distance with a non-holonomic robot," in *Proc. of the 2005 IEEE/RSJ Int. Conf. on Intelligent Robots and Systems*, Atizapan, Mexico, Aug. 2005, pp. 2687–2693.
[19] R. Murrieta-Cid, R. Monroy, S. Hutchinson, and J.-P. Laumond, "A complexity result for the pursuit-evasion game of maintaining visibility of a moving evader," in *Proc. of the 2008 IEEE Int. Conf. on Robotics and Automation*, Pasadena, CA, May 2008, pp. 2657–2664.
[20] R. Murrieta-Cid, T. Muppirala, A. Sarmiento, S. Bhattacharya, and S. Hutchinson, "Surveillance strategies for a pursuer with finite sensor range," *The Int. Journal of Robotics Research*, vol. 26, no. 3, pp. 233–253, Mar. 2007.
[21] J.-P. Aubin, *Viability Theory*. Birkhäuser, 1991.
[22] D. Panagou, H. G. Tanner, and K. J. Kyriakopoulos, "Dipole-like fields for stabilization of systems with Pfaffian constraints," in *Proc. of the 2010 IEEE Int. Conf. on Robotics and Automation*, Anchorage, Alaska, May 2010, pp. 4499–4504.
[23] L. Bushnell, B. Mirtich, A. Sahai, and M. Secor, "Off-tracking bounds for a car pulling trailers with kingpin hitching," in *Proc. of the 33th IEEE Conference on Decision and Control*, Lake Buena Vista, FL, USA, Dec. 1994, pp. 2944–2949.
[24] D. Panagou and V. Kumar, "Maintaining visibility for leader-follower formations in obstacle environments," in *Proc. of the 2012 IEEE Int. Conf. on Robotics and Automation*, St. Paul, Minnesota, USA, May 2012, pp. 1811–1816.
[25] D. Panagou and K. J. Kyriakopoulos, "Viability control for a class of underactuated systems," *Automatica*, vol. 49, no. 1, pp. 17–29, Jan. 2013.
[26] H. K. Khalil, *Nonlinear Systems. 3rd Edition*. Prentice-Hall Inc., 2002.
[27] S. M. LaValle, *Planning Algorithms*. Cambridge University Press, 2006.
[28] F. Blanchini and S. Miani, *Set-Theoretic Methods in Control*. Birkhäuser, 2008.
[29] J.-P. Aubin and H. Frankowska, *Set-valued Analysis*. Birkhäuser, 1990.
[30] S. R. Lindemann and S. M. LaValle, "Simple and efficient algorithms for computing smooth, collision-free feedback laws over given cell decompositions," *The Int. Journal of Robotics Research*, vol. 28, no. 5, pp. 600–621, 2009.
[31] D. Liberzon, *Switching in Systems and Control*. Birkhäuser, 2003.

Dimitra Panagou received her Diploma in Mechanical Engineering (February 2006) and her Ph.D. in Engineering (April 2012) from the School of Mechanical Engineering, National Technical University of Athens, Greece.

Her research interests mainly lie within the fields of motion planning, coordination and multi-objective control of robotic systems (mobile, marine, aerial), with emphasis on the use and development of set-theoretic control methods, in order to address real world constrained control problems via analytic, provably correct solutions. She is particularly interested in the control design for single- and multi-agent systems which are subject to motion constraints, underactuation, restricted sensing and communication capabilities and additive disturbances.

In the past, Dr. Panagou has been a Visiting Research Scholar at the Mechanical Engineering Department, University of Delaware (Spring semester 2009) and at the GRASP Laboratory, School of Engineering and Applied Science, University of Pennsylvania (June 2013, Fall semester 2010), while since August 2012 she has joined the Coordinated Science Laboratory, University of Illinois at Urbana-Champaign, as a Postdoctoral Research Associate.

Vijay Kumar is the UPS Foundation Professor in the School of Engineering and Applied Science at the University of Pennsylvania, and on sabbatical leave at White House Office of Science and Technology Policy where he serves as the assistant director for robotics and cyber physical systems. He received his Bachelors of Technology from the Indian Institute of Technology, Kanpur and his Ph.D. from The Ohio State University in 1987. He has been on the Faculty in the Department of Mechanical Engineering and Applied Mechanics with a secondary appointment in the Department of Computer and Information Science at the University of Pennsylvania since 1987.

Dr. Kumar served as the Deputy Dean for Research in the School of Engineering and Applied Science from 2000-2004. He directed the GRASP Laboratory, a multidisciplinary robotics and perception laboratory, from 1998-2004. He was the Chairman of the Department of Mechanical Engineering and Applied Mechanics from 2005-2008. He then served as the Deputy Dean for Education in the School of Engineering and Applied Science from 2008-2012.

Dr. Kumar is a Fellow of the American Society of Mechanical Engineers (2003), a Fellow of the Institution of Electrical and Electronic Engineers (2005) and a member of the National Academy of Engineering (2013).

Dr. Kumar's research interests are in robotics, specifically multi-robot systems, and micro aerial vehicles. He has served on the editorial boards of the IEEE Transactions on Robotics and Automation, IEEE Transactions on Automation Science and Engineering, ASME Journal of Mechanical Design, the ASME Journal of Mechanisms and Robotics and the Springer Tract in Advanced Robotics (STAR). He is the recipient of the 1991 National Science Foundation Presidential Young Investigator award, the 1996 Lindback Award for Distinguished Teaching (University of Pennsylvania), the 1997 Freudenstein Award for significant accomplishments in mechanisms and robotics, the 2012 ASME Mechanisms and Robotics Award, the 2012 IEEE Robotics and Automation Society Distinguished Service Award and a 2012 World Technology Network Award. He has won best paper awards at DARS 2002, ICRA 2004, ICRA 2011, RSS 2011, and RSS 2013, and has advised doctoral students who have won Best Student Paper Awards at ICRA 2008, RSS 2009, and DARS 2010.

APPENDIX A
PROOF OF THEOREM 1

Proof: Let us consider the continuously differentiable function V in terms of the position errors $x_1 = x - x_d$, $y_1 = y - y_d$ and the orientation error $\eta = \beta - \varphi$, as:

$$V = V_1 + \frac{1}{2}(\beta-\varphi)^2 = \frac{1}{2}\left({x_1}^2 + {y_1}^2\right) + \frac{1}{2}(\beta-\varphi)^2,$$

and take its time derivative along the system trajectories as:

$$\begin{aligned}\dot{V} &\overset{(7)}{=} x_1(u_\mathrm{F}\cos\beta - u_\mathrm{L} + y w_\mathrm{L}) + y_1(u_\mathrm{F}\sin\beta - x w_\mathrm{L}) + \\ &+ (\beta-\varphi)(w_\mathrm{F} - w_\mathrm{L} - \dot{\varphi}) = \left[\begin{smallmatrix} x_1 & y_1 \end{smallmatrix}\right]\begin{bmatrix}\cos\beta \\ \sin\beta\end{bmatrix} u_\mathrm{F} + \\ &+ \left[\begin{smallmatrix} x_1 & y_1 & \beta-\varphi \end{smallmatrix}\right]\begin{bmatrix} -u_\mathrm{L}+y w_\mathrm{L} \\ -x w_\mathrm{L} \\ -w_\mathrm{L}\end{bmatrix} + (\beta-\varphi)(w_\mathrm{F} - \dot{\varphi}) = \\ &\overset{(12b)}{=} \underbrace{\boldsymbol{r}_1^\top \begin{bmatrix}\cos\beta \\ \sin\beta\end{bmatrix} u_\mathrm{F} + \boldsymbol{q}_1^\top \boldsymbol{g}(\boldsymbol{q}, \boldsymbol{v_L})}_{P(\boldsymbol{q}_1)} - k_2(\beta-\varphi)^2,\end{aligned}$$

where $\boldsymbol{r_1} = \begin{bmatrix} x_1 & y_1 \end{bmatrix}^\top$, $\boldsymbol{q_1} = \begin{bmatrix} \boldsymbol{r_1}^\top & \beta-\varphi \end{bmatrix}^\top$. The dynamics of the orientation error $\eta = \beta - \varphi$ read: $\dot{\eta} = \dot{\beta} - \dot{\varphi} \Rightarrow \dot{\eta} = w_\mathrm{F} - w_\mathrm{L} - \dot{\varphi} \Rightarrow \dot{\eta} = -k_2\eta - w_\mathrm{L}$. If $w_\mathrm{L} = 0$, it follows that $\eta \to 0$ exponentially, i.e. that $\beta \to \varphi$. However, w_L is not in general equal to zero. Let us assume that w_L is *slowly-varying*, i.e. that w_L is continuously differentiable and $\|\dot{w}_\mathrm{L}\|$ is sufficiently small [26]. Then, w_L can be treated as a frozen parameter, and the frozen system $0 = -k_2\eta - w_\mathrm{L}$ has a continuously differentiable isolated root $\eta = -\frac{1}{k_2}w_\mathrm{L} = h(w_\mathrm{L})$, for which $\|\frac{\partial h}{\partial w_\mathrm{L}}\| = \frac{1}{k_2}$ is bounded. To analyze the stability properties of the frozen equilibrium $z = \eta + \frac{1}{k_2}w_\mathrm{L}$, take $\dot{z} = -k_2(z - \frac{1}{k_2}w_\mathrm{L}) - w_\mathrm{L} = -k_2 z$. Then, z is exponentially stable, i.e. $\eta \to -\frac{1}{k_2}w_\mathrm{L}$. The term $P(\boldsymbol{q}_1)$ in $\dot{V}$ then reads:

$$\begin{aligned}P(\boldsymbol{q}_1) &\overset{(12a)}{=} -k_1\left|\boldsymbol{r_1}^\top\begin{bmatrix}\cos\beta \\ \sin\beta\end{bmatrix}\right|\|\boldsymbol{r_1}\| - \\ &- \mathrm{sgn}(\boldsymbol{p}^\top\boldsymbol{r_1})\; u_\mathrm{L}^\star\; \boldsymbol{r_1}^\top\begin{bmatrix}\cos\beta \\ \sin\beta\end{bmatrix} + \boldsymbol{q}_1^\top\boldsymbol{g}(\boldsymbol{q}, \boldsymbol{v_L}),\end{aligned}$$

where $\boldsymbol{q}_1^\top\boldsymbol{g}(\boldsymbol{q}, \boldsymbol{v_L}) = -x_1 u_\mathrm{L} + \left[\begin{smallmatrix} x_1 & y_1 \end{smallmatrix}\right]\left[\begin{smallmatrix} y \\ -x \end{smallmatrix}\right] w_\mathrm{L} - (\beta-\varphi)w_\mathrm{L}$. For $\eta = -\frac{1}{k_2}w_\mathrm{L}$ one has: $\boldsymbol{q}_1^\top\boldsymbol{g}(\boldsymbol{q}, \boldsymbol{v_L}) = -x_1 u_\mathrm{L} + \frac{1}{k_2}{w_\mathrm{L}}^2$, since $\left[\begin{smallmatrix} x_1 & y_1 \end{smallmatrix}\right]\left[\begin{smallmatrix} y \\ -x \end{smallmatrix}\right] = 0$. This is further written as:

$$\boldsymbol{q}_1^\top\boldsymbol{g}(\boldsymbol{q}, \boldsymbol{v_L}) = \left[\begin{smallmatrix} x_1 & y_1 \end{smallmatrix}\right]\left[\begin{smallmatrix} -u_\mathrm{L} \\ 0 \end{smallmatrix}\right] + \frac{{w_\mathrm{L}}^2}{k_2} \le \|\boldsymbol{r_1}\|u_\mathrm{L}^\star + \frac{{w_\mathrm{L}}^2}{k_2}.$$

To check the signum of $P(\boldsymbol{q}_1)$, consider the following cases:
C1. $\mathrm{sgn}(\boldsymbol{p}^\top\boldsymbol{r_1}) = -1$ and $\boldsymbol{r_1}^\top\begin{bmatrix}\cos\beta \\ \sin\beta\end{bmatrix} < 0$. Then:

$$\begin{aligned}P(\boldsymbol{q}_1) &= -\left|\boldsymbol{r_1}^\top\begin{bmatrix}\cos\beta \\ \sin\beta\end{bmatrix}\right|(k_1\|\boldsymbol{r_1}\| + u_\mathrm{L}^\star) + \boldsymbol{q}_1^\top\boldsymbol{g}(\boldsymbol{q}, \boldsymbol{v_L}) \\ &\le -\left|\boldsymbol{r_1}^\top\begin{bmatrix}\cos\beta \\ \sin\beta\end{bmatrix}\right|(k_1\|\boldsymbol{r_1}\| + u_\mathrm{L}^\star) + \|\boldsymbol{r_1}\|u_\mathrm{L}^\star + \frac{{w_\mathrm{L}}^2}{k_2}.\end{aligned}$$

The term $P(\boldsymbol{q}_1)$ is < 0 if:

$$\begin{aligned}\left|\boldsymbol{r_1}^\top\begin{bmatrix}\cos\beta \\ \sin\beta\end{bmatrix}\right|(k_1\|\boldsymbol{r_1}\| + u_\mathrm{L}^\star) > \|\boldsymbol{r_1}\|u_\mathrm{L}^\star + \frac{{w_\mathrm{L}}^2}{k_2} \Rightarrow \\ k_1\|\boldsymbol{r_1}\|^2 + \|\boldsymbol{r_1}\|u_\mathrm{L}^\star > \|\boldsymbol{r_1}\|u_\mathrm{L}^\star + \frac{{w_\mathrm{L}}^2}{k_2} \Rightarrow \\ \|\boldsymbol{r_1}\|^2 > \frac{{w_\mathrm{L}}^2}{k_1 k_2} \Rightarrow \|\boldsymbol{r_1}\| > \frac{|w_\mathrm{L}|}{\sqrt{k_1 k_2}}. \qquad (22)\end{aligned}$$

Note that (22) is sufficient, not necessary.
C2. $\mathrm{sgn}(\boldsymbol{p}^\top\boldsymbol{r_1}) = -1$ and $\boldsymbol{r_1}^\top\begin{bmatrix}\cos\beta \\ \sin\beta\end{bmatrix} \ge 0$.

This case corresponds to configurations such that L is not visible to F, and thus we may drop it since it is not relevant to the problem considered here.
C3. $\mathrm{sgn}(\boldsymbol{p}^\top\boldsymbol{r_1}) = 1$ and $\boldsymbol{r_1}^\top\begin{bmatrix}\cos\beta \\ \sin\beta\end{bmatrix} > 0$. Then:

$$P(\boldsymbol{q}_1) = -\left|\boldsymbol{r_1}^\top\begin{bmatrix}\cos\beta \\ \sin\beta\end{bmatrix}\right|(k_1\|\boldsymbol{r_1}\| + u_\mathrm{L}^\star) + \boldsymbol{q}_1^\top\boldsymbol{g}(\boldsymbol{q}, \boldsymbol{v_L}),$$

and the analysis for ensuring that $P(\boldsymbol{q}_1) < 0$ follows the same pattern as in **C1**, yielding the sufficient condition (22).
C4. $\mathrm{sgn}(\boldsymbol{p}^\top\boldsymbol{r_1}) = 1$ and $\boldsymbol{r_1}^\top\begin{bmatrix}\cos\beta \\ \sin\beta\end{bmatrix} \le 0$. This case can be dropped for the same reasoning in **C2**.

In summary, one has $P(\boldsymbol{q}_1) < 0$ for any $\boldsymbol{r_1}$ that satisfies (22) yielding $\dot{V} = P(\boldsymbol{q}_1) - k_2(\beta-\varphi)^2 < 0$. Consequently, for any initial $\boldsymbol{r_1}(0)$ and any $0 < \epsilon_r < \|\boldsymbol{r_1}(0)\|$ that satisfies (22), $\dot{V}$ is negative in the set $\left\{\boldsymbol{r_1} \;\middle|\; \frac{1}{2}{\epsilon_r}^2 \le V(\|\boldsymbol{r_1}\|) \le \frac{1}{2}\|\boldsymbol{r_1}(0)\|^2\right\}$, which verifies that $\boldsymbol{r_1}(t)$ enters the set $\left\{\boldsymbol{r_1} \;\middle|\; V(\boldsymbol{r_1}) \le \frac{1}{2}{\epsilon_r}^2\right\}$, or equivalently, $\boldsymbol{r_1}(t)$ enters the ball $\mathcal{B}(\boldsymbol{0}, \epsilon_r)$. Equivalently, if ϵ_r is chosen to satisfy (22), the system trajectories $\boldsymbol{r}(t)$ enter and remain into the ball $\mathcal{B}(\boldsymbol{r_d}, \epsilon_r)$. ■

APPENDIX B
WHEN BOTH VISIBILITY CONSTRAINTS ARE ACTIVE

Let us assume that the system starts on an initial configuration so that L lies at point A (Fig. 3) where: $\phi = \alpha$,

$$x^2 + y^2 = {L_s}^2,\; y = L_s\sin(\beta+\alpha),\; x = L_s\cos(\beta+\alpha).$$

The derivative $\dot{h}_1(\cdot)$ of the first visibility constraint reads:

$$\begin{aligned}\dot{h}_1 &= \left[-\tfrac{y}{x^2+y^2} \quad \tfrac{x}{x^2+y^2} \quad -1\right]\begin{bmatrix} u_\mathrm{F}\cos\beta - u_\mathrm{L} + y w_\mathrm{L} \\ u_\mathrm{F}\sin\beta - x w_\mathrm{L} \\ w_\mathrm{F} - w_\mathrm{L}\end{bmatrix} = \\ &= \frac{u_\mathrm{F}}{x^2+y^2}(x\sin\beta - y\cos\beta) - w_\mathrm{F} + \frac{y u_\mathrm{L}}{x^2+y^2}.\end{aligned}$$

After some algebra, condition (13) for $k = 1$ reduces into:

$$-u_\mathrm{F}\sin\alpha\tan\alpha + u_\mathrm{L}\sin(\beta+\alpha)\tan\alpha < w_\mathrm{F}L_s\tan\alpha. \quad (23)$$

The derivative $\dot{h}_2(\cdot)$ of the second visibility constraint reads:

$$\begin{aligned}\dot{h}_2 = \tfrac{u_\mathrm{F}}{\sqrt{x^2+y^2}}\left(\left[\begin{smallmatrix} x & y \end{smallmatrix}\right]\begin{bmatrix}\cos\beta \\ \sin\beta\end{bmatrix} + \tfrac{L_s\cos\alpha\tan\phi}{\sqrt{x^2+y^2}\cos\phi}\left[\begin{smallmatrix} x & y \end{smallmatrix}\right]\begin{bmatrix}-\sin\beta \\ \cos\beta\end{bmatrix}\right) + \\ - \tfrac{L_s\cos\alpha\tan\phi}{\cos\phi}w_\mathrm{F} - \tfrac{u_\mathrm{L}}{\sqrt{x^2+y^2}}\left(x - \tfrac{y L_s\cos\alpha\tan\phi}{\sqrt{x^2+y^2}\cos\phi}\right).\end{aligned}$$

After some algebra, condition (13) for $k = 2$ reduces into:

$$\begin{aligned}-u_\mathrm{L}(\cos(\beta+\alpha) - \sin(\beta+\alpha)\tan\alpha) + \\ + u_\mathrm{F}(\cos\alpha - \tan\alpha\sin\alpha) < w_\mathrm{F}L_s\tan\alpha. \qquad (24)\end{aligned}$$

Then, visibility is maintained as long as the gains k_1, k_2 in (12) are chosen so that both (23), (24) hold. These reduce into:

$$u_\mathrm{F} > \frac{u_\mathrm{L}\; f(\beta,\alpha)}{g(\alpha)}, \quad w_\mathrm{F} > \frac{u_\mathrm{F}\; g(\alpha) - u_\mathrm{L}\; f(\beta,\alpha)}{L_s\tan\alpha},$$

where:

$$\begin{aligned}f(\beta,\alpha) &\triangleq \cos(\beta+\alpha) - \sin(\beta+\alpha)\tan\alpha, \\ g(\alpha) &\triangleq \cos\alpha - \sin\alpha\tan\alpha.\end{aligned}$$

Take $0 < \alpha < \frac{\pi}{4}$, which yields $g(\alpha) > 0$, and denote $f(\beta^\star, \alpha)$ the maximum (positive) value of the function $f(\cdot, \alpha)$, obtained

for the worst-case initial orientation $\beta^\star$. Note also that the values of the control laws (12) for the system initiating at point A are: $u_{\rm F} = k_1(L_s - r_d) + u_{\rm L}^\star$, $w_{\rm F} = k_2\alpha$. Then:

$$k_1 > \frac{u_{\rm L}^\star \left(\frac{f(\beta^\star,\alpha)}{g(\alpha)} - 1\right)}{L_s - r_d},\ k_2 > \frac{k_1(L_s - r_d)g(\alpha) - u_{\rm L}^\star f(\beta^\star,\alpha)}{\alpha L_s \tan\alpha}.$$

Similarly one can treat the case for $\alpha > \frac{\pi}{4}$, as well as for the system initiating on the point B (Fig. 2).

Remark 6: The conditions (23), (24) refer to the worst-case initial configurations (i.e. on the boundary of the visibility set K where both constraints are active). Therefore, their satisfaction is sufficient for ensuring visibility maintenance from any other initial configuration in K as well.

APPENDIX C
CELL DECOMPOSITION

We perform a cell decomposition into convex polygonal cells *by extending the boundaries of each static obstacle until intersecting with another obstacle or the external boundary of the workspace*, see Fig. 12(a). For the corridor environment considered here the resulting cells are rectangular.

Given an initial and a final configuration for L, marked with "**o**" and "**x**" respectively, one may find or define a high-level discrete motion plan indicating the sequence of cells i that L has to go through; here we have $i \in \{1, 2, \ldots, 11\}$, while the goal destination lies in cell 12 (Fig. 12(a)).

On the common face between two successive cells i, $i+1$ we draw the orthogonal vector pointing into cell $i+1$, see the red vectors in Fig. 12(a). These denote the desired direction of motion of L when transiting from cell i to cell $i+1$.

To reduce the number of cells we merge successive cells whose red vectors are parallel; thus, cells $2, 3$ in Fig. 12(a) are merged into cell 2 in Fig. 12(b), and so on. In the sequel, we work with the cell decomposition depicted in Fig. 12(b). The same logic applies also in more complex

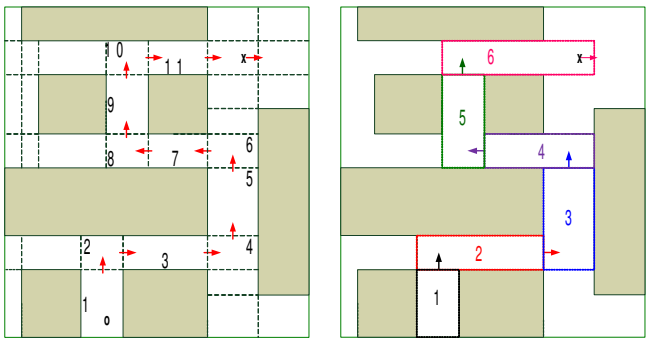

(a) The initial cell decomposition. (b) Reducing the number of cells.

Fig. 12. The considered cell decomposition in corridor environments.

polygonal environments, i.e. in the case of obstacles with arbitrary convex shape (Fig. 13).

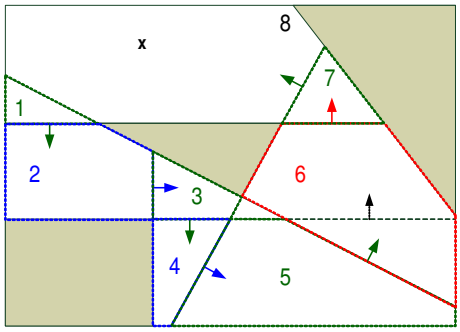

Fig. 13. The considered cell decomposition in polygonal environments.